Search for supersymmetric particles assuming R-parity non-conservation in e^+e^- collisions at $\sqrt{s}$ = 192 to 208 GeV

J. Abdallah, P. Abreu, W. Adam, T. Albrecht, T. Alderweireld, R. Alemany-Fernandez, T. Allmendinger, P. Allport, U. Amaldi, N. Amapane, et al.

▶ **To cite this version:**

J. Abdallah, P. Abreu, W. Adam, T. Albrecht, T. Alderweireld, et al.. Search for supersymmetric particles assuming R-parity non-conservation in e^+e^- collisions at $\sqrt{s}$ = 192 to 208 GeV. European Physical Journal C: Particles and Fields, 2004, 36, pp.1-23. ⟨10.1140/epjc/s2004-01881-6⟩. ⟨in2p3-00022155⟩

HAL Id: in2p3-00022155

https://in2p3.hal.science/in2p3-00022155v1

Submitted on 9 Aug 2004

HAL is a multi-disciplinary open access archive for the deposit and dissemination of scientific research documents, whether they are published or not. The documents may come from teaching and research institutions in France or abroad, or from public or private research centers.

L'archive ouverte pluridisciplinaire **HAL**, est destinée au dépôt et à la diffusion de documents scientifiques de niveau recherche, publiés ou non, émanant des établissements d'enseignement et de recherche français ou étrangers, des laboratoires publics ou privés.

HAL Authorization

arXiv:hep-ex/0406009 v2 4 Jun 2004

EUROPEAN ORGANIZATION FOR NUCLEAR RESEARCH

CERN–EP/2003-092

23 September 2003

Search for supersymmetric particles assuming R–parity non-conservation in e^+e^- collisions at $\sqrt{s} = 192$ to 208 GeV

DELPHI Collaboration

Abstract

Searches for pair-production of supersymmetric particles under the assumption of non-conservation of R–parity with a dominant $LL\bar{E}$ or $\bar{U}\bar{D}\bar{D}$ term have been performed using the data collected by the DELPHI experiment at LEP in e^+e^- collisions at centre-of-mass energies from 192 up to 208 GeV. No excess of data above Standard Model expectations was observed. The results were used to constrain the MSSM parameter space and to derive limits on the masses of supersymmetric particles.

(Accepted by Eur. Phys. J. C)

J.Abdallah[25], P.Abreu[22], W.Adam[51], P.Adzic[11], T.Albrecht[17], T.Alderweireld[2], R.Alemany-Fernandez[8], T.Allmendinger[17], P.P.Allport[23], U.Amaldi[29], N.Amapane[45], S.Amato[48], E.Anashkin[36], A.Andreazza[28], S.Andringa[22], N.Anjos[22], P.Antilogus[25], W-D.Apel[17], Y.Arnoud[14], S.Ask[26], B.Asman[44], J.E.Augustin[25], A.Augustinus[8], P.Baillon[8], A.Ballestrero[46], P.Bambade[20], R.Barbier[27], D.Bardin[16], G.J.Barker[17], A.Baroncelli[39], M.Battaglia[8], M.Baubillier[25], K-H.Becks[53], M.Begalli[6], A.Behrmann[53], E.Ben-Haim[20], N.Benekos[32], A.Benvenuti[5], C.Berat[14], M.Berggren[25], L.Berntzon[44], D.Bertrand[2], M.Besancon[40], N.Besson[40], D.Bloch[9], M.Blom[31], M.Bluj[52], M.Bonesini[29], M.Boonekamp[40], P.S.L.Booth[23], G.Borisov[21], O.Botner[49], B.Bouquet[20], T.J.V.Bowcock[23], I.Boyko[16], M.Bracko[43], R.Brenner[49], E.Brodet[35], P.Bruckman[18], J.M.Brunet[7], L.Bugge[33], P.Buschmann[53], M.Calvi[29], T.Camporesi[8], V.Canale[38], F.Carena[8], N.Castro[22], F.Cavallo[5], M.Chapkin[42], Ph.Charpentier[8], P.Checchia[36], R.Chierici[8], P.Chliapnikov[42], J.Chudoba[8], S.U.Chung[8], K.Cieslik[18], P.Collins[8], R.Contri[13], G.Cosme[20], F.Cossutti[47], M.J.Costa[50], D.Crennell[37], J.Cuevas[34], J.D'Hondt[2], J.Dalmau[44], T.da Silva[48], W.Da Silva[25], G.Della Ricca[47], A.De Angelis[47], W.De Boer[17], C.De Clercq[2], B.De Lotto[47], N.De Maria[45], A.De Min[36], L.de Paula[48], L.Di Ciaccio[38], A.Di Simone[39], K.Doroba[52], J.Drees[53,8], M.Dris[32], G.Eigen[4], T.Ekelof[49], M.Ellert[49], M.Elsing[8], M.C.Espirito Santo[22], G.Fanourakis[11], D.Fassouliotis[11,3], M.Feindt[17], J.Fernandez[41], A.Ferrer[50], F.Ferro[13], U.Flagmeyer[53], H.Foeth[8], E.Fokitis[32], F.Fulda-Quenzer[20], J.Fuster[50], M.Gandelman[48], C.Garcia[50], Ph.Gavillet[8], E.Gazis[32], R.Gokieli[8,52], B.Golob[43], G.Gomez-Ceballos[41], P.Goncalves[22], E.Graziani[39], G.Grosdidier[20], K.Grzelak[52], J.Guy[37], C.Haag[17], A.Hallgren[49], K.Hamacher[53], K.Hamilton[35], S.Haug[33], F.Hauler[17], V.Hedberg[26], M.Hennecke[17], H.Herr[8], J.Hoffman[52], S-O.Holmgren[44], P.J.Holt[8], M.A.Houlden[23], K.Hultqvist[44], J.N.Jackson[23], G.Jarlskog[26], P.Jarry[40], D.Jeans[35], E.K.Johansson[44], P.D.Johansson[44], P.Jonsson[27], C.Joram[8], L.Jungermann[17], F.Kapusta[25], S.Katsanevas[27], E.Katsoufis[32], G.Kernel[43], B.P.Kersevan[8,43], U.Kerzel[17], A.Kiiskinen[15], B.T.King[23], N.J.Kjaer[8], P.Kluit[31], P.Kokkinias[11], C.Kourkoumelis[3], O.Kouznetsov[16], Z.Krumstein[16], M.Kucharczyk[18], J.Lamsa[1], G.Leder[51], F.Ledroit[14], L.Leinonen[44], R.Leitner[30], J.Lemonne[2], V.Lepeltier[20], T.Lesiak[18], W.Liebig[53], D.Liko[51], A.Lipniacka[44], J.H.Lopes[48], J.M.Lopez[34], D.Loukas[11], P.Lutz[40], L.Lyons[35], J.MacNaughton[51], A.Malek[53], S.Maltezos[32], F.Mandl[51], J.Marco[41], R.Marco[41], B.Marechal[48], M.Margoni[36], J-C.Marin[8], C.Mariotti[8], A.Markou[11], C.Martinez-Rivero[41], J.Masik[12], N.Mastroyiannopoulos[11], F.Matorras[41], C.Matteuzzi[29], F.Mazzucato[36], M.Mazzucato[36], R.Mc Nulty[23], C.Meroni[28], E.Migliore[45], W.Mitaroff[51], U.Mjoernmark[26], T.Moa[44], M.Moch[17], K.Moenig[8,10], R.Monge[13], J.Montenegro[31], D.Moraes[48], S.Moreno[22], P.Morettini[13], U.Mueller[53], K.Muenich[53], M.Mulders[31], L.Mundim[6], W.Murray[37], B.Muryn[19], G.Myatt[35], T.Myklebust[33], M.Nassiakou[11], F.Navarria[5], K.Nawrocki[52], R.Nicolaidou[40], M.Nikolenko[16,9], A.Oblakowska-Mucha[19], V.Obraztsov[42], A.Olshevski[16], A.Onofre[22], R.Orava[15], K.Osterberg[15], A.Ouraou[40], A.Oyanguren[50], M.Paganoni[29], S.Paiano[5], J.P.Palacios[23], H.Palka[18], Th.D.Papadopoulou[32], L.Pape[8], C.Parkes[24], F.Parodi[13], U.Parzefall[8], A.Passeri[39], O.Passon[53], L.Peralta[22], V.Perepelitsa[50], A.Perrotta[5], A.Petrolini[13], J.Piedra[41], L.Pieri[39], F.Pierre[40], M.Pimenta[22], E.Piotto[8], T.Podobnik[43], V.Poireau[8], M.E.Pol[6], G.Polok[18], V.Pozdniakov[16], N.Pukhaeva[2,16], A.Pullia[29], J.Rames[12], A.Read[33], P.Rebecchi[8], J.Rehn[17], D.Reid[31], R.Reinhardt[53], P.Renton[35], F.Richard[20], J.Ridky[12], M.Rivero[41], D.Rodriguez[41], A.Romero[45], P.Ronchese[36], P.Roudeau[20], T.Rovelli[5], V.Ruhlmann-Kleider[40], D.Ryabtchikov[42], A.Sadovsky[16], L.Salmi[15], J.Salt[50], C.Sander[17], A.Savoy-Navarro[25], U.Schwickerath[8], A.Segar[35], R.Sekulin[37], M.Siebel[53], A.Sisakian[16], G.Smadja[27], O.Smirnova[26], A.Sokolov[42], A.Sopczak[21], R.Sosnowski[52], T.Spassov[8], M.Stanitzki[17], A.Stocchi[20], J.Strauss[51], B.Stugu[4], M.Szczekowski[52], M.Szeptycka[52], T.Szumlak[19], T.Tabarelli[29], A.C.Taffard[23], F.Tegenfeldt[49], J.Timmermans[31], L.Tkatchev[16], M.Tobin[23], S.Todorovova[12], B.Tome[22], A.Tonazzo[29], P.Tortosa[50], P.Travnicek[12], D.Treille[8], G.Tristram[7], M.Trochimczuk[52], C.Troncon[28], M-L.Turluer[40], I.A.Tyapkin[16], P.Tyapkin[16], S.Tzamarias[11], V.Uvarov[42], G.Valenti[5], P.Van Dam[31], J.Van Eldik[8], A.Van Lysebetten[2], N.van Remortel[2], I.Van Vulpen[8], G.Vegni[28], F.Veloso[22], W.Venus[37], P.Verdier[27], V.Verzi[38], D.Vilanova[40], L.Vitale[47], V.Vrba[12], H.Wahlen[53], A.J.Washbrook[23], C.Weiser[17], D.Wicke[8],

J.Wickens[2], G.Wilkinson[35], M.Winter[9], M.Witek[18], O.Yushchenko[42], A.Zalewska[18], P.Zalewski[52], D.Zavrtanik[43], V.Zhuravlov[16], N.I.Zimin[16], A.Zintchenko[16], M.Zupan[11]

[1]Department of Physics and Astronomy, Iowa State University, Ames IA 50011-3160, USA
[2]Physics Department, Universiteit Antwerpen, Universiteitsplein 1, B-2610 Antwerpen, Belgium
and IIHE, ULB-VUB, Pleinlaan 2, B-1050 Brussels, Belgium
and Faculté des Sciences, Univ. de l'Etat Mons, Av. Maistriau 19, B-7000 Mons, Belgium
[3]Physics Laboratory, University of Athens, Solonos Str. 104, GR-10680 Athens, Greece
[4]Department of Physics, University of Bergen, Allégaten 55, NO-5007 Bergen, Norway
[5]Dipartimento di Fisica, Università di Bologna and INFN, Via Irnerio 46, IT-40126 Bologna, Italy
[6]Centro Brasileiro de Pesquisas Físicas, rua Xavier Sigaud 150, BR-22290 Rio de Janeiro, Brazil
and Depto. de Física, Pont. Univ. Católica, C.P. 38071 BR-22453 Rio de Janeiro, Brazil
and Inst. de Física, Univ. Estadual do Rio de Janeiro, rua São Francisco Xavier 524, Rio de Janeiro, Brazil
[7]Collège de France, Lab. de Physique Corpusculaire, IN2P3-CNRS, FR-75231 Paris Cedex 05, France
[8]CERN, CH-1211 Geneva 23, Switzerland
[9]Institut de Recherches Subatomiques, IN2P3 - CNRS/ULP - BP20, FR-67037 Strasbourg Cedex, France
[10]Now at DESY-Zeuthen, Platanenallee 6, D-15735 Zeuthen, Germany
[11]Institute of Nuclear Physics, N.C.S.R. Demokritos, P.O. Box 60228, GR-15310 Athens, Greece
[12]FZU, Inst. of Phys. of the C.A.S. High Energy Physics Division, Na Slovance 2, CZ-180 40, Praha 8, Czech Republic
[13]Dipartimento di Fisica, Università di Genova and INFN, Via Dodecaneso 33, IT-16146 Genova, Italy
[14]Institut des Sciences Nucléaires, IN2P3-CNRS, Université de Grenoble 1, FR-38026 Grenoble Cedex, France
[15]Helsinki Institute of Physics, P.O. Box 64, FIN-00014 University of Helsinki, Finland
[16]Joint Institute for Nuclear Research, Dubna, Head Post Office, P.O. Box 79, RU-101 000 Moscow, Russian Federation
[17]Institut für Experimentelle Kernphysik, Universität Karlsruhe, Postfach 6980, DE-76128 Karlsruhe, Germany
[18]Institute of Nuclear Physics PAN,Ul. Radzikowskiego 152, PL-31142 Krakow, Poland
[19]Faculty of Physics and Nuclear Techniques, University of Mining and Metallurgy, PL-30055 Krakow, Poland
[20]Université de Paris-Sud, Lab. de l'Accélérateur Linéaire, IN2P3-CNRS, Bât. 200, FR-91405 Orsay Cedex, France
[21]School of Physics and Chemistry, University of Lancaster, Lancaster LA1 4YB, UK
[22]LIP, IST, FCUL - Av. Elias Garcia, 14-1^{o}, PT-1000 Lisboa Codex, Portugal
[23]Department of Physics, University of Liverpool, P.O. Box 147, Liverpool L69 3BX, UK
[24]Dept. of Physics and Astronomy, Kelvin Building, University of Glasgow, Glasgow G12 8QQ
[25]LPNHE, IN2P3-CNRS, Univ. Paris VI et VII, Tour 33 (RdC), 4 place Jussieu, FR-75252 Paris Cedex 05, France
[26]Department of Physics, University of Lund, Sölvegatan 14, SE-223 63 Lund, Sweden
[27]Université Claude Bernard de Lyon, IPNL, IN2P3-CNRS, FR-69622 Villeurbanne Cedex, France
[28]Dipartimento di Fisica, Università di Milano and INFN-MILANO, Via Celoria 16, IT-20133 Milan, Italy
[29]Dipartimento di Fisica, Univ. di Milano-Bicocca and INFN-MILANO, Piazza della Scienza 2, IT-20126 Milan, Italy
[30]IPNP of MFF, Charles Univ., Areal MFF, V Holesovickach 2, CZ-180 00, Praha 8, Czech Republic
[31]NIKHEF, Postbus 41882, NL-1009 DB Amsterdam, The Netherlands
[32]National Technical University, Physics Department, Zografou Campus, GR-15773 Athens, Greece
[33]Physics Department, University of Oslo, Blindern, NO-0316 Oslo, Norway
[34]Dpto. Fisica, Univ. Oviedo, Avda. Calvo Sotelo s/n, ES-33007 Oviedo, Spain
[35]Department of Physics, University of Oxford, Keble Road, Oxford OX1 3RH, UK
[36]Dipartimento di Fisica, Università di Padova and INFN, Via Marzolo 8, IT-35131 Padua, Italy
[37]Rutherford Appleton Laboratory, Chilton, Didcot OX11 OQX, UK
[38]Dipartimento di Fisica, Università di Roma II and INFN, Tor Vergata, IT-00173 Rome, Italy
[39]Dipartimento di Fisica, Università di Roma III and INFN, Via della Vasca Navale 84, IT-00146 Rome, Italy
[40]DAPNIA/Service de Physique des Particules, CEA-Saclay, FR-91191 Gif-sur-Yvette Cedex, France
[41]Instituto de Fisica de Cantabria (CSIC-UC), Avda. los Castros s/n, ES-39006 Santander, Spain
[42]Inst. for High Energy Physics, Serpukov P.O. Box 35, Protvino, (Moscow Region), Russian Federation
[43]J. Stefan Institute, Jamova 39, SI-1000 Ljubljana, Slovenia and Laboratory for Astroparticle Physics,
Nova Gorica Polytechnic, Kostanjeviska 16a, SI-5000 Nova Gorica, Slovenia,
and Department of Physics, University of Ljubljana, SI-1000 Ljubljana, Slovenia
[44]Fysikum, Stockholm University, Box 6730, SE-113 85 Stockholm, Sweden
[45]Dipartimento di Fisica Sperimentale, Università di Torino and INFN, Via P. Giuria 1, IT-10125 Turin, Italy
[46]INFN,Sezione di Torino, and Dipartimento di Fisica Teorica, Università di Torino, Via P. Giuria 1,
IT-10125 Turin, Italy
[47]Dipartimento di Fisica, Università di Trieste and INFN, Via A. Valerio 2, IT-34127 Trieste, Italy
and Istituto di Fisica, Università di Udine, IT-33100 Udine, Italy
[48]Univ. Federal do Rio de Janeiro, C.P. 68528 Cidade Univ., Ilha do Fundão BR-21945-970 Rio de Janeiro, Brazil
[49]Department of Radiation Sciences, University of Uppsala, P.O. Box 535, SE-751 21 Uppsala, Sweden
[50]IFIC, Valencia-CSIC, and D.F.A.M.N., U. de Valencia, Avda. Dr. Moliner 50, ES-46100 Burjassot (Valencia), Spain
[51]Institut für Hochenergiephysik, Österr. Akad. d. Wissensch., Nikolsdorfergasse 18, AT-1050 Vienna, Austria
[52]Inst. Nuclear Studies and University of Warsaw, Ul. Hoza 69, PL-00681 Warsaw, Poland
[53]Fachbereich Physik, University of Wuppertal, Postfach 100 127, DE-42097 Wuppertal, Germany

1 Introduction

The R–parity (R_p) symmetry plays an essential role in the construction of supersymmetric theories, such as the Minimal Supersymmetric extension of the Standard Model (MSSM) [1]. The conservation of R_p is closely related to the conservation of lepton (L) and baryon (B) numbers and the multiplicative quantum number associated to the R_p symmetry is defined by $R_p = (-1)^{3B+L+2S}$ for a particle with spin S [2]. Standard model particles have even R_p, whereas the corresponding superpartners have odd R_p. The conservation of R_p guarantees that the spin–0 sfermions cannot be directly exchanged between standard fermions. It also implies that the sparticles ($R_p = -1$) can only be produced in pairs, and that the decay of a sparticle leads to another sparticle, or an odd number of them. Therefore, it ensures the stability of the Lightest Supersymmetric Particle (LSP). In the MSSM, the conservation of R_p is assumed: this is phenomenologically justified by proton decay constraints, and by the fact that a neutral LSP could be a good dark matter candidate.

From a theoretical point of view, the conservation of R_p is not mandatory in supersymmetric extensions of the Standard Model (SM). Nevertheless, to be in agreement with the present experimental limit on proton lifetime, R_p violation can be introduced in MSSM either via the non-conservation of L or the non-conservation of B. One of the major consequences of the non-conservation of R_p is the allowed decay of the LSP into fermions; this modifies the signatures of supersymmetric particle production compared to the expected signatures in the case of R_p conservation.

In this paper, searches for pair-produced supersymmetric particles in the hypothesis of R_p violation via one dominant sparticle-particle coupling are presented. The data recorded in 1999 and 2000 by the DELPHI experiment have been analyzed, and no signal of R_p-violating decays was found in any of the channels. Previous results published by DELPHI on this subject can be found in references [3,4]. Similar searches performed by the other three LEP experiments have also shown no evidence for R_p-violating effects [5].

The paper is organized as follows. Section 2 is dedicated to the R_p violation phenomenology considered in the present search. The data samples and simulated sets are presented in Section 3. Section 4 is devoted to the description of the analyses, and in Section 5 the search results are given and interpreted in order to constrain the mass spectrum of SUSY particles. A brief summary is given in the last section.

2 R_p non-conservation framework

In the presence of R_p violation the superpotential [6] contains three trilinear terms, two violating L conservation, and one violating B conservation. We consider here the $\lambda_{ijk}\mathrm{L}_i\mathrm{L}_j\bar{\mathrm{E}}_k$ (non-conservation of L) and $\lambda''_{ijk}\bar{\mathrm{U}}_i\bar{\mathrm{D}}_j\bar{\mathrm{D}}_k$ (non-conservation of B) terms [1], which couple the sleptons to the leptons and the squarks to the quarks, respectively. Since $\lambda_{ijk} = -\lambda_{jik}$ and $\lambda''_{ijk} = -\lambda''_{ikj}$, due to SU(2) and SU(3) symmetries, there are only 9 λ_{ijk} and only 9 λ''_{ijk} free couplings. In the present work, it is assumed that only one λ_{ijk} or λ''_{ijk} is dominant at a time. In the following, searches assuming R_p-violation via one dominant $\lambda_{ijk}\mathrm{L}_i\mathrm{L}_j\bar{\mathrm{E}}_k$ term are referred as "LL$\bar{\mathrm{E}}$", and those via one $\lambda''_{ijk}\bar{\mathrm{U}}_i\bar{\mathrm{D}}_j\bar{\mathrm{D}}_k$ term as "$\bar{\mathrm{U}}\bar{\mathrm{D}}\bar{\mathrm{D}}$". Searches assuming R_p-violation via one $\lambda'_{ijk}\mathrm{L}_i\mathrm{Q}_j\bar{\mathrm{D}}_k$ term (non-conservation of L) were not performed in DELPHI for data collected in 1999 and 2000.

[1] i, j, k are generation indices, L denotes the lepton doublet superfields, $\bar{E}$ ($\bar{U}$, $\bar{D}$) denote the lepton (up and down quark) singlet superfields, λ_{ijk} and λ''_{ijk} are Yukawa couplings.

In the pair-production of supersymmetric particles studied here, R_p is not conserved in the decay of the sparticles, but is conserved at the production vertex. The production cross-sections behave as in the MSSM with R_p conservation (see section 2.3).

2.1 R_p-violating decays of sparticles via LL$\bar{\text{E}}$ or $\bar{\text{U}}\bar{\text{D}}\bar{\text{D}}$ terms

Two types of supersymmetric particle decays are considered: *direct decay* and *indirect decay*.

2.1.1 Direct decays

R_p violation allows the direct decay of a sfermion into two conventional fermions (Fig. 1–a, b), or the direct decay of a neutralino or a chargino into a fermion and a virtual sfermion which then decays into two conventional fermions (Fig. 1–c). A direct decay is the only possibility for the LSP.

Decays through LL$\bar{\text{E}}$ terms

Sleptons are coupled to leptons through the $\lambda_{ijk}\text{L}_i\text{L}_j\bar{\text{E}}_k$ term. In four-component Dirac notation, the LL$\bar{\text{E}}$ Yukawa interaction terms are[2] [7]:

$$\lambda_{ijk}\left(\tilde{\nu}_{iL}\bar{\ell}_{kR}\ell_{jL} + \tilde{\ell}_{jL}\bar{\ell}_{kR}\nu_{iL} + \tilde{\ell}^*_{kR}(\overline{\nu}_{iL})^c\tilde{\ell}_{jL} - i \leftrightarrow j\right) + \text{h.c.}$$

Considering the above expression, it can be deduced that the R_p-violating decay of a sfermion is possible only with specific indices i, j, k of the coupling which is considered to be dominant. The possible sparticle decays with such a dominant λ_{ijk} coupling are listed below.

- The sneutrino direct decay gives two charged leptons: via λ_{ijk} only the $\tilde{\nu}_i$ and $\tilde{\nu}_j$ are allowed to decay directly: $\tilde{\nu}_i \rightarrow \ell^{\pm}_{jL}\ell^{\mp}_{kR}$ and $\tilde{\nu}_j \rightarrow \ell^{\pm}_{iL}\ell^{\mp}_{kR}$ respectively.
- The charged slepton direct decay gives one neutrino and one charged lepton (the lepton flavour may be different from the slepton one). Among the supersymmetric partners of the right-handed leptons, only the one belonging to the k^{th} generation can decay directly: $\tilde{\ell}^-_{kR} \rightarrow \nu_{iL}\ell^-_{jL}$, $\ell^-_{iL}\nu_{jL}$. For the supersymmetric partners of the left-handed leptons, the allowed direct decays are: $\tilde{\ell}^-_{iL} \rightarrow \bar{\nu}_{jL}\ell^-_{kR}$ and $\tilde{\ell}^-_{jL} \rightarrow \bar{\nu}_{iL}\ell^-_{kR}$.
- The neutralino decays via a virtual slepton and a lepton, and subsequently gives three-lepton final states (two charged leptons and one neutrino):
  $\widetilde{\chi}^0 \rightarrow \ell^+_i\bar{\nu}_j\ell^-_k$, $\ell^-_i\nu_j\ell^+_k$, $\bar{\nu}_i\ell^+_j\ell^-_k$, $\nu_i\ell^-_j\ell^+_k$.
- The chargino decays via a virtual slepton and gives either three charged leptons, or two neutrinos and one charged lepton:
  $\widetilde{\chi}^+_1 \rightarrow \ell^+_i\ell^+_j\ell^-_k$, $\ell^+_i\bar{\nu}_j\nu_k$, $\bar{\nu}_i\ell^+_j\nu_k$, $\nu_i\nu_j\ell^+_k$.

Decays through $\bar{\text{U}}\bar{\text{D}}\bar{\text{D}}$ terms

The squarks are coupled to the quarks through the $\lambda''_{ijk}\bar{\text{U}}_i\bar{\text{D}}_j\bar{\text{D}}_k$ term. The decays allowed via this term can be inferred by considering the Lagrangian for the trilinear Yukawa interactions written in expanded notation:

$$\lambda''_{ijk}\left(\overline{(\text{u}_\text{i})^\text{c}}\ \overline{(\text{d}_\text{j})^\text{c}}\widetilde{\text{d}}^*_k + \overline{(\text{u}_\text{i})^\text{c}}\ \widetilde{\text{d}}^*_j\ \overline{(\text{d}_\text{k})^\text{c}} + \widetilde{\text{u}}^*_i\ \overline{(\text{d}_\text{j})^\text{c}}\ \overline{(\text{d}_\text{k})^\text{c}}\right) + \text{h.c.}$$

From this Lagrangian, we can derive the following rules:

[2]Here ν ($\tilde{\nu}$) refer to neutrino (sneutrino) fields, ℓ ($\tilde{\ell}$) refer to charged lepton (slepton) fields, i,j,k are generation indices and the superfix c refers to a charge-conjugate field.

- The direct decays of squarks into two quarks are given by: $\widetilde{\mathrm{u}}_{i,R} \rightarrow \bar{\mathrm{d}}_{j,R}\bar{\mathrm{d}}_{k,R}$, $\widetilde{\mathrm{d}}_{j,R} \rightarrow \bar{\mathrm{u}}_{i,R}\bar{\mathrm{d}}_{k,R}$ and $\widetilde{\mathrm{d}}_{k,R} \rightarrow \bar{\mathrm{u}}_{i,R}\bar{\mathrm{d}}_{j,R}$.
- The neutralino decays via a virtual squark and a quark and subsequently gives a three-quark final state:
  $\widetilde{\chi}^0 \rightarrow \bar{\mathrm{u}}_j\bar{\mathrm{d}}_j\bar{\mathrm{d}}_k$, $\mathrm{u}_j\mathrm{d}_j\mathrm{d}_k$
- Chargino decay is similar to the neutralino one, and then gives also a three quarks final state: $\widetilde{\chi}_1^+ \rightarrow \mathrm{u}_j\mathrm{d}_j\mathrm{u}_k$, $\mathrm{u}_i\mathrm{u}_j\mathrm{d}_k$, $\bar{\mathrm{d}}_i\bar{\mathrm{d}}_j\bar{\mathrm{d}}_k$

2.1.2 Indirect decays

Indirect decays are cascade decays through R_p-conserving vertices to on-shell supersymmetric particles, down to the lightest supersymmetric particle, which then decays via one $\mathrm{LL\bar{E}}$ or $\mathrm{\bar{U}\bar{D}\bar{D}}$ term (Fig. 2). A typical example is the R_p-conserving decay $\tilde{\chi}_1^+ \rightarrow \tilde{\chi}_1^0 + \mathrm{W}^{*+}$ (see Fig. 2–e) and the subsequent decay of $\tilde{\chi}_1^0$ through the R_p-violating couplings. The indirect decay mode usually dominates when there is enough phase space available in the decay between "mother" and "daughter" sparticles. For example, when the difference of masses between these two sparticles is larger than 5–10 GeV/c^2. Regions of the parameter space where there is a "dynamic" suppression of the R_p-conserving modes also exist. In this case, even if the sparticle is not the LSP, it decays through an R_p-violating mode. For example, if the field component of the two lightest neutralinos is mainly the photino, then the decay $\widetilde{\chi}_2^0 \rightarrow \widetilde{\chi}_1^0\ \mathrm{Z}^*$ is suppressed.

The sfermion indirect decay studied here is the decay through the lightest neutralino considered as the LSP ($\tilde{\mathrm{f}} \rightarrow \mathrm{f}'\ \widetilde{\chi}_1^0$), followed by the R_p-violating decay of the LSP. With $\mathrm{LL\bar{E}}$, the indirect decay of a sneutrino (charged slepton) through a neutralino and a neutrino (charged lepton) leads to two charged leptons and two neutrinos (three charged leptons and one neutrino). The squark decay into a quark and a gaugino leads to one quark and three leptons. With $\mathrm{\bar{U}\bar{D}\bar{D}}$, the indirect decay of a squark (slepton) leads to four quarks (three quarks and one lepton).

2.2 R_p-violating coupling upper limits and LSP lifetime

Upper limits on the λ_{ijk} and λ''_{ijk} couplings can be derived mainly from indirect searches of R_p-violating effects [7,8], assuming that only one coupling is dominant at a time. They are dependent on the sfermion mass, and usually given for $\mathrm{m}_{\tilde{\mathrm{f}}} = 100$ GeV/c^2. The upper bounds on λ_{ijk} are obtained from charged-current universality, lepton universality, ν_μ–e scattering, forward-backward asymmetry in $\mathrm{e^+e^-}$ collisions, and bounds on ν_e–Majorana mass. Most present indirect limits are in the range of 10^{-3} to 10^{-1}; the most stringent upper limit is given for λ_{133} ($\simeq 6 \cdot 10^{-3}$). Upper limits on λ''_{ijk} couplings come from experimental measurements of double nucleon decays for λ''_{112} (10^{-6}), $n - \bar{n}$ oscillations for λ''_{113} (10^{-5}) and of $R_\ell = \Gamma_{had}(\mathrm{Z}^0)/\Gamma_\ell(\mathrm{Z}^0)$ in $\mathrm{e^+e^-}$ collisions for $\lambda''_{312}, \lambda''_{313}, \lambda''_{323}$ (0.43). The upper limits on the other λ''_{ijk} couplings are obtained from the requirement of perturbative unification at the Grand Unified Theory (GUT) scale of 10^{16} GeV. This gives a limit of 1.25.

In the present searches, the LSP lifetime was a crucial parameter since the analyses were valid only if the R_p-violating decays were close to the production vertex, which means a LSP flight path shorter than a few centimetres.

The LSP mean decay length is given by [9,10]:

$$\mathrm{L(cm)} = 0.3\ (\beta\gamma) \left(\frac{\mathrm{m_{\tilde{f}}}}{100\ \mathrm{GeV/c^2}} \right)^4 \left(\frac{1\ \mathrm{GeV/c^2}}{\mathrm{m_{\widetilde{\chi}}}} \right)^5 \frac{1}{\Lambda^2} \qquad (1)$$

if the neutralino or the chargino is the LSP with $\beta\gamma = \mathrm{P_{\widetilde{\chi}}}/\mathrm{m_{\widetilde{\chi}}}$ and with $\Lambda = \lambda_{ijk}$ or $\Lambda = \sqrt{3}\lambda''_{ijk}$. Considering the upper limits on the couplings described above and according to equation (1), the analyses are not sensitive to a light neutralino ($\mathrm{m_{\chi}} \leq 15\ \mathrm{GeV}/c^2$), due to the terms $\mathrm{m_{\widetilde{\chi}}}^{-5}$ and $(\beta\gamma)$. Moreover, when studying neutralino decays, for the typical masses considered in the present study, the analyses are sensitivite to R_p-violating couplings greater than 10^{-4} to 10^{-5}, where the R_p-violating decay has a negligible decay length. For much lower values of the coupling strength, the LSP escapes the tracking devices before decaying and the results of the searches performed under the assumption of R_p conservation are recovered [11]. Between these two extreme cases, the LSP decay produces a displaced vertex topology [3].

2.3 Pair-production of supersymmetric particles

Pair-production of supersymmetric particles in the MSSM assuming R_p violation is identical to pair-production in the case of R_p conservation, since the trilinear couplings are not present at the production vertex. The production of single supersymmetric particles via trilinear couplings has been studied in other searches performed by the DELPHI collaboration [13].

In the constrained MSSM scheme [1] considered in the present searches, the mass spectrum of neutralinos and charginos is determined by three parameters, with the assumption that both the gaugino and the sfermion masses are unified at the GUT scale. The relevant parameters are then: $\mathrm{M_2}$, the SU(2) gaugino mass at the electroweak scale (it is assumed that $\mathrm{M_1} = \frac{5}{3}\tan^2\theta_{\mathrm{W}}\mathrm{M_2}$), $\mathrm{m_0}$, the common sfermion mass at the GUT scale, μ, the mass-mixing term of the Higgs doublets at the electroweak scale and $\tan\beta$, the ratio of the vacuum expectation values of the two Higgs doublets. It is assumed that the running of the λ_{ijk} and λ''_{ijk} couplings from the GUT to the electroweak scales does not have a significant effect on the "running" of the gaugino and sfermion masses.

The charginos are produced in pairs in the s-channel via γ or Z exchange, or in the t-channel via $\widetilde{\nu}_{\mathrm{e}}$ exchange if the charginos have a gaugino component; the neutralinos are produced in pairs via s-channel Z exchange provided they have a higgsino component, or via t-channel $\tilde{\mathrm{e}}$ exchange if they have a gaugino component. The t-channel contribution is suppressed when the slepton masses (depending on $\mathrm{m_0}$) are high enough. When the $\tilde{\mathrm{e}}$ mass is sufficiently small (less than $100\ \mathrm{GeV}/c^2$), neutralino production can be enhanced, because of the t-channel contribution. On the contrary, if the $\widetilde{\nu}_{\mathrm{e}}$ mass is in the same range, the chargino cross-section can decrease due to destructive interference between the s- and t-channel amplitudes.

The pair-production cross-section of sfermions mainly depends on the sfermion masses. The $\tilde{\mathrm{e}}$ and $\widetilde{\nu}_{\mathrm{e}}$ cross-sections are also very sensitive to the neutralino and chargino compositions (which are function of μ, $\mathrm{M_2}$ and $\tan\beta$) via the t-channel exchange. The sfermion mass-eigenstates, $\tilde{\mathrm{f}}_1$ and $\tilde{\mathrm{f}}_2$ (where f is a quark or lepton and $\tilde{\mathrm{f}}_1$ is lighter than $\tilde{\mathrm{f}}_2$), are

[3] This particuliar topology, not considered in the present searches, has been studied in other searches performed by the DELPHI collaboration [12].

obtained from the two supersymmetric scalar partners $\tilde{f}_L$ and $\tilde{f}_R$ of the corresponding left and right-handed fermion [14,15]:

$$\begin{aligned} \tilde{f}_1 &= \tilde{f}_L \cos\Phi_{\rm mix} + \tilde{f}_R \sin\Phi_{\rm mix} \\ \tilde{f}_2 &= -\tilde{f}_L \sin\Phi_{\rm mix} + \tilde{f}_R \cos\Phi_{\rm mix} \end{aligned}$$

where $\Phi_{\rm mix}$ is the mixing angle with $0 \leq \Phi_{\rm mix} \leq \pi$. The supersymmetric partner of the left-handed fermions are likely to be heavier than their right-handed counterparts. The $\tilde{f}_L$–$\tilde{f}_R$ mixing is related to the off-diagonal terms of the scalar squared-mass matrix. It is proportional to the fermion mass, and is small compared to the diagonal terms, with the possible exception of the third family sfermion [16]. The lighter stop, $\tilde{t}_1$, is then probably the lightest squark. This is not only due to the mixing effect but also to the effect of the large Yukawa coupling of the top; both tend to decrease the mass of $\tilde{t}_1$ [17]. Similarly the lightest charged slepton is probably the $\tilde{\tau}_1$. For small values of tanβ, $\tilde{\tau}_1$ is predominantly a $\tilde{\tau}_R$, and it is not so much lighter than $\tilde{e}_1$ and $\tilde{\mu}_1$. In the present slepton search, a no-mixing scenario is assumed. In the third squark generation searches two left-right mixing angle cases have been considered. The first one with mixing angle equal to zero and the second one with the mixing angle $\Phi_{\rm mix} = 56^\circ$ ($\Phi_{\rm mix} = 68^\circ$) corresponding to the minimum production cross-section of the stop (sbottom) via Z exchange [18].

3 Data and generated samples

3.1 Data samples

The data recorded in 1999 and 2000 by the DELPHI experiment at centre-of-mass energies from $\sqrt{s} = 192$ GeV to 208.8 GeV, correspond to a total integrated luminosity of around 450 pb^{-1}. The DELPHI detector has been described elsewhere [19]. An integrated luminosity of 386 pb^{-1} (Table 1) has been analysed, corresponding to high quality data, with the tracking detectors and the electromagnetic calorimeters in good working conditions. At the end of the data taking period in 2000, one sector (among twelve) of the Time Projection Chamber (TPC) failed beyond repair. This required modifications in the data treatment (pattern recognition), and a specific simulation of the detector with one TPC sector off has been performed. An integrated luminosity of 51.8 pb^{-1} recorded with one TPC sector off have been analysed.

3.2 Event generators

To evaluate background contaminations, different contributions coming from the SM processes were considered. The SM events were produced by the following generators:

- $\gamma\gamma$ events: `BDK` [20] for $\gamma\gamma \to \ell^+\ell^-$ processes, including radiative corrections for the $e^+e^-\mu^+\mu^-$ and $e^+e^-\tau^+\tau^-$ final states, and `TWOGAM` for $\gamma\gamma \to$ hadron processes.
- two-fermion processes: `BHWIDE` [21] for Bhabha scattering ($e^+e^- \to e^+e^-(\gamma)$), `KORALZ` [22] for $e^+e^- \to \mu^+\mu^-(\gamma)$ and for $e^+e^- \to \tau^+\tau^-(\gamma)$ and `PYTHIA 6.143` [23] for $e^+e^- \to q\bar{q}(\gamma)$ events.
- four-fermion processes: `EXCALIBUR` [24] and `GRC4F` [25] for all types of four-fermion processes: non resonant ($f\bar{f}f'\bar{f}'$), singly resonant ($Zf\bar{f}$, $Wf\bar{f}'$) and doubly resonant (ZZ, WW) (`PYTHIA` was used also for cross-checks on the final results).

Signal events were generated for all analyses with the `SUSYGEN 3.00` program [26].

All generated background and signal events were passed through the full DELPHI simulation and reconstruction chain [19] and then processed in the same way as the real

data. To treat the data taken with one sector of the TPC off, special background and signal event samples were generated, and the same treatment applied to them as to the real data.

3.3 Signal samples

Choice of the R_p-violating couplings

Among the nine λ_{ijk} couplings, λ_{122} (which leads to several muons in the final states) and λ_{133} (which leads to several taus in the final states) have been chosen for most of the signal generation. Their values were set for $m_{\tilde{\ell}} = 100$ GeV/c^2 at 0.04 and 0.003 respectively, below their upper bound derived from indirect searches of R_p-violating effects. Any value between 10^{-3} and 10^{-1} would not change the neutralino decay topologies. Simulations with other couplings have been also performed in order to check that the analyses developed for λ_{122} or λ_{133} were able to select the corresponding signal with an equal or better efficiency.

For the generation of all $\bar{\mathrm{U}}\bar{\mathrm{D}}\bar{\mathrm{D}}$ signals, a λ''_{212} coupling of strength 0.1 (for $m_{\tilde{q}} = 100$ GeV/c^2) was used. Any value between 10^{-2} and 0.5 would not change the neutralino decay topologies.

Searches for decays through specific λ''_{ijk} couplings, leading to the production of one or several b quarks, can use b–tagging techniques to reach higher sensitivities, but at the cost of losing generality.

Generated signal sets

Two different procedures were applied to the signal generation for gaugino pair-production and subsequent decays through either $\mathrm{LL\bar{E}}$ or $\bar{\mathrm{U}}\bar{\mathrm{D}}\bar{\mathrm{D}}$ terms in order to cover the MSSM parameter space.

For the $\mathrm{LL\bar{E}}$ term, the $\widetilde{\chi}_i^0$ and $\widetilde{\chi}_k^{\pm}$ pair-production processes were considered for different values of tanβ (from 1 to 30), m_0 (between 90 GeV/c^2 and 500 GeV/c^2), μ (between –200 GeV/c^2 and 200 GeV/c^2) and M_2 (between 5 and 400 GeV/c^2), for centre-of-mass energies of 200 and 206 GeV. For the $\bar{\mathrm{U}}\bar{\mathrm{D}}\bar{\mathrm{D}}$ term, pair-production of neutralinos was generated for several masses. The simulated masses started from 10 GeV/c^2 and were increased in steps of 10 GeV/c^2, as long as the mass of the chargino remained kinematically accessible. Masses corresponding to the kinematic limit were also simulated. To generate chargino pairs, the mass of the chargino was varied from 45 GeV/c^2 to 95 GeV/c^2 with a 10 GeV/c^2 step. Chargino masses were also simulated at the kinematic limit. The neutralino mass was varied from 10 GeV/c^2 to a mass difference with the chargino of 5 GeV/c^2 with a 10 GeV/c^2 step. For each mass pair, a set of the variables μ, M_2 and tanβ was found for the chosen simulation.

Sfermion indirect decay signals were simulated at different masses with steps of 10 GeV/c^2 at centre-of-mass energies of 200 and 206 GeV, with tanβ and μ fixed at 1.5 and –200 GeV/c^2 respectively. M_2 was used to fix the neutralino mass at the required value. The points were simulated from 45 to 100 GeV/c^2 for the sfermion masses and from 15 to 95 GeV/c^2 for the $\widetilde{\chi}_1^0$ masses up to a mass difference between the sfermion and the LSP of 5 GeV/c^2.

Among the sfermions, only the sneutrino direct decay via $\mathrm{LL\bar{E}}$ terms was studied. Specific signal sets have been produced with $\mathrm{Br}(\tilde{\nu} \rightarrow \ \ell^+\ell^-) = 100\%$. The processes

$\widetilde{\nu}_e\widetilde{\bar{\nu}}_e \to 4\mu$ (λ_{122}), $\widetilde{\nu}_e\widetilde{\bar{\nu}}_e \to 4\tau$ (λ_{133}), $\widetilde{\nu}_\mu\widetilde{\bar{\nu}}_\mu \to 4\tau$ (λ_{233}) and $\widetilde{\nu}_\tau\widetilde{\bar{\nu}}_\tau \to 2e2\tau$ (λ_{133}) have been generated for different values of the sneutrino mass up to 98 GeV/c^2, with tanβ and μ fixed at 1.5 and –200 GeV/c^2 respectively. In order to check that all final states from $\tilde{\nu}\tilde{\bar{\nu}}$ decay were covered, signals obtained for other λ_{ijk} couplings and for sneutrino masses around 90 GeV/c^2 were also generated.

4 Description of the analyses

The analyses covering the decay of pair-produced sparticles were designed to cover multi-lepton final states for $LL\bar{E}$ coupling and multi-jet final states for $\bar{U}\bar{D}\bar{D}$ coupling. Different preselections were applied, one for the multi-lepton channels and one for the multi-jet channels. In each case, dedicated analyses were necessary to take into account the specific characteristics of the sparticle decay. The multi-jet analyses required a specific treatment based on neural network techniques.

The sensitivity of the searches for sparticle indirect decays depended on the mass difference (ΔM) between the sparticle being searched for and the LSP. The analyses were designed to be efficient for $\Delta M \geq 5$ GeV/c^2. The multi-jet analyses required different signal selection optimisations to cover efficiently all ΔM regions; therefore they were divided into windows according to the value of ΔM.

No excess in the data appeared in these searches, therefore a working point optimization on the selection criteria was performed minimizing the expected excluded cross-section as a function of the average signal efficiency.

4.1 Description of the final states

4.1.1 Decays via $LL\bar{E}$

Direct and indirect decays of gauginos, direct and indirect decays of sneutrinos and indirect decays of charged sleptons and squarks were studied.

The direct decay of a pair of lightest neutralinos leads to two neutrinos and four charged leptons. For an indirect decay of chargino or heavier neutralino pairs the final state may contain some jets and/or leptons in addition to the four leptons and the missing energy from the decay of the LSP. The direct decay of a sneutrino pair gives final states with four charged leptons, in which the leptons can be of two different flavours. The direct decay of a charged slepton pair gives final states with two charged leptons, in which the leptons can be of two different flavours, and missing energy. This final state has not been covered by the present analyses. In the indirect decay of any sfermion pair, the final states are composed of two fermions plus the decay products of the neutralinos.

Compared to other couplings the highest efficiencies and background reduction were obtained in analyses performed on the signal with a dominant λ_{122} coupling. For analyses dedicated to a λ_{133} coupling, due to the presence of several taus in the decay channels, the efficiencies and the rejection power were low. For final states produced by other λ_{ijk}, the detection efficiencies lay between these two limiting cases. Therefore conservative limits can be derived by considering the results of the analyses performed assuming a dominant λ_{133} coupling, and only these analyses will be described in section 4.3.

The decay of pair-produced sparticles via a λ_{133} coupling leads to different types of final states, depending on the produced sparticles. The $\widetilde{\chi}_1^0\widetilde{\chi}_1^0$ decay via λ_{133} leads to $2\tau + \ell + \ell' + \not{E}$, where $\ell, \ell' =$ e or τ, and $\not{E}$ means missing energy. In addition, jets and/or leptons from the W or Z decays show up in the final state from $\widetilde{\chi}_i^0\widetilde{\chi}_j^0$ and $\widetilde{\chi}_1^+\widetilde{\chi}_1^-$ indirect

decays. The indirect decay of a slepton pair gives $2\tau + \ell + \ell' + \not{E}$, with two additional charged leptons (same flavour, opposite charge) in the case of charged sleptons, and additional missing energy in the case of sneutrinos. A 4τ final state is produced by the direct decay of $\widetilde{\nu}_e\widetilde{\bar{\nu}}_e$ via λ_{133}. The direct decay of $\widetilde{\nu}_\tau\widetilde{\bar{\nu}}_\tau$ gives 2e2τ and then, there is finally less missing energy comming from the taus decay than in the previous cases. The indirect decay of squarks adds exactly two jets to the $2\tau + \ell + \ell' + \not{E}$.

Four analyses have been performed to search for all these topologies. They are summarized in the first part of Table 2.

4.1.2 Decays via $\bar{U}\bar{D}\bar{D}$

Direct and indirect decays of gauginos, and indirect decays of charginos, charged sleptons and squarks were studied.

For each indirect decay of a chargino, squark or slepton pair there are at least six quarks in the final state. Therefore the most important feature of these decays is the number of quarks produced, which can be up to ten for the indirect decay of two charginos with the hadronic decays of the W bosons. The indirect decay channel presents the only possibility for the sleptons to decay through a $\bar{U}\bar{D}\bar{D}$ term. In this case, two leptons are produced in the R_p conserving decay of the slepton pair, and they add to the six jets coming from the decay of the two neutralinos: a 6 jets + 2ℓ, ℓ = e, μ final state is the signature of these signals. The indirect decay of a stop or sbottom pair produces 8 jets in the final state. Two b quarks are produced from the sbottom decay. The analysis of the different decay channels was organized on the basis of the number of hadronic jets in the final state (see Table 2).

4.2 Analysis tools and techniques

4.2.1 Lepton identification

The identification of a muon or an electron, used in all λ_{ijk} analyses and several λ''_{ijk} ones, was based on standard DELPHI algorithms [19]. The identification could be "tight" if it was an unambiguous one, or "loose" otherwise. In the multi-lepton analyses described in this section a particle was considered as a well identified electron if it satisfied the tight conditions from the DELPHI electron identification algorithm, its momentum was greater than 8 GeV/c and there was no other charged particle in a cone of half-angle 2° around it. A particle was considered as a well identified muon if its momentum was greater than 5 GeV/c and it was tagged as a tight muon candidate by the DELPHI algorithm.

4.2.2 Jet reconstruction algorithms

Two different jet reconstruction algorithms have been used. The `DURHAM` algorithm [27] was used for the multi-lepton ($LL\bar{E}$ coupling) analyses, where jets were expected from τ or W boson decays. In case of multi-jet analyses, the `CAMBRIDGE` clustering algorithm [28] implemented in the `CKERN` package [29] was used.

The `CAMBRIDGE` algorithm was introduced to select soft jets, coming from quark-jets with gluon emission. The specific procedure of clusterization which extracts soft jets from the list of objects to be clustered, was particularly interesting for multi-jet analyses, where the jets (more than six) may not be well separated in momentum space. For each event, the two algorithms provided all possible configurations of jets between 2 and

10. They have the same definition of y_{cut} distance, but mainly differ in the iterative procedure of clustering. In this paper, the transition value of the y_{cut} in the DURHAM or CAMBRIDGE algorithm at which the event changes from a clustering with n jets, called n-jet configuration, to a clustering with $(n-1)$-jets, is denoted y_{nn-1}. In other words, the y_{nn-1} value is the y_{cut} value for which the number of particle clusters flips from n to $n-1$ for increasing y_{cut} distances. For example, the y_{43} value of one event is the highest value of y_{cut} to obtain 4 separated clusters of particles.

4.2.3 Neural networks

A neural network method was applied in order to distinguish signals from SM background events for all multi-jet analyses. The trainings of the neural networks were done in the standard back-propagation manner with one hidden layer on samples of simulated background ($q\bar{q}$ and four-fermion) and signal events. A feed-forward algorithm has been implemented to compute from the input discriminating variables a single discriminant variable (signal output node) which was used first to validate the training with different signal and background samples and then to select the final number of candidate events for each analysis. The exact configuration and the input discriminating variables of each neural network depended on the search channel. The working point on the signal ouput node value has been chosen to minimize the expected excluded cross-section at 95% confidence level (CL) when there is no signal.

4.3 Multi-lepton LL$\bar{\text{E}}$ channels

4.3.1 Preselection

The selections were based on the criteria already presented in [3], using mainly missing momentum, lepton identification and kinematic properties. The preselection requirements were:

- more than three charged particles and at least one of them with a polar angle between 40° and 140°;
- at least one identified lepton (e or μ);
- a total energy greater than $0.1 \cdot \sqrt{s}$;
- a missing momentum component transverse to the beam (p_t) greater than 5 GeV/c;
- a polar angle of the missing momentum (θ_{miss}) between 27° and 153°;
- a thrust axis not close to the beam pipe, viz. $|\cos\theta_{th}|$ less than 0.9;
- an acollinearity[4] greater than 2°, and greater than 7° for events with a charged particle multiplicity greater than 6.

The preselection was efficient in suppressing 99.9% of the backgrounds coming from Bhabha scattering and two-photon processes while removing 97% of the $f\bar{f}(\gamma)$ contribution. The preselection also reduced the four-fermion contamination by 75%. After this preselection stage, 2310 events (1220 for data at centre-of-mass energies between 192 and 202 GeV, and 1090 for those collected above 202 GeV) were selected to be compared to 2254 ± 6 expected from the background sources (1189 ± 5 at centre-of-mass energies between 192 and 202 GeV, 1065 ± 4 above 202 GeV). The corresponding efficiencies for the large majority of LL$\bar{\text{E}}$ signals lay between 60% and 80%. The distributions of several event variables at the hadronic preselection stage are shown in Figure 3.

The above requirements had to be slightly modified for the stop analysis (see Section 4.3.5), in particular to take into account the fact that the final state always contains two

[4]The acollinearity is computed between the two vectors corresponding to the sum of the particle momenta in each hemisphere of the event. The two hemispheres are defined by the plane orthogonal to the thrust axis.

jets. A minimum multiplicity of eight charged particles was required. No requirement was applied on the thrust axis. On the other hand, a stronger cut was applied on the polar angle of the missing momentum ($30^\circ \leq \theta_{\rm miss} \leq 150^\circ$). After this preselection stage, 2197 events were selected to be compared to 2208 $\pm$ 6 expected from the background sources.

4.3.2 Gaugino search

The gaugino analysis was designed to cover the $2\tau + n\ell + mj + \not{E}$ ($n \geq 2$, $m \geq 0$) final states, from direct or indirect decays of gauginos, and to be efficient for both low and high multiplicity cases.

The thrust had to be less than 0.9 and a lower limit on the missing energy was applied viz. $E_{\rm miss}$ greater than $0.3 \cdot \sqrt{s}$. The number of neutral (charged) particles had to be less than 20 (25) and the polar angle of at least one lepton had to be between 40° and 140°.

The events were then separated in to two classes, according to their charged particle multiplicity.

- For events with a charged particle multiplicity from four to six, (mainly for neutralino direct decay topologies), the following criteria were applied:
  - the energy in a cone of 30° around the beam axis was required to be less than 50% of the total visible energy;
  - the energy of the most energetic lepton (e or μ) had to be between 2 and 70 GeV;
  - there should be no other charged particle in a cone of half angle of 20° (6°) around any identified lepton for a charged particle multiplicity equal to 4 (5 or 6).
- For events with a charged particle multiplicity greater than six, the previous criteria became:
  - the energy in a cone of 30° around the beam axis was required to be less than 40% of the total visible energy;
  - the energy of the most energetic lepton had to be between 5 and 60 GeV,
  - if there was only one identified lepton; there should be no other charged particle in a cone with a half angle of 6° around it; if there was more than one identified lepton there should be no other charged particle in a cone with a half angle of 10° around at least two of them;
  - at least one electron (loose identification) was required.

These criteria removed 95% of $f\bar{f}\gamma$, ZZ and W^+W^- events.

A selection based on the jet characteristics and topologies was then applied, depending on the charged particle multiplicity, as mentioned above. First, constraints were imposed on the y_{32} and y_{43} values: they had to be greater than 0.002 and 0.0001 respectively for events with low charged particle multiplicity, and greater than 0.016 and 0.005 respectively for events whose charged particle multiplicity was above 7; these criteria eliminated 99% of the remaining $f\bar{f}\gamma$ contribution. In events with more than six charged particles, it was required that at least one jet had no more than two charged particles. In four or five-jet configurations, a minimum number of 4 jets with at least one charged particle was required. For a four-jet topology, a cut was applied on the value of $E^j_{\rm min} \cdot \theta_{\rm min}$ where $E^j_{\rm min}$ is the energy of the least energetic jet, and $\theta_{\rm min}$ is the minimum di-jet angle (Fig. 4–a). It had to be greater than 1 GeV·rad for events with low charged particle multiplicity, and greater then 5 GeV·rad for events with a charged particle multiplicity above 7. These requirements reduced the background from 4-fermion processes.

4.3.3 Slepton search

A slepton analysis, aimed to search for $2\tau + 2\ell + \not{E}$ $(+ 2\ell)$ was performed in order to study the following three channels:

- $\tilde{\ell}^+_R\tilde{\ell}^-_R \rightarrow \ell\widetilde{\chi}^0_1\ell\widetilde{\chi}^0_1$;
- $\tilde{\nu}\bar{\tilde{\nu}} \rightarrow \nu\widetilde{\chi}^0_1\nu\widetilde{\chi}^0_1$;
- $\widetilde{\nu}_e\bar{\widetilde{\nu}}_e \rightarrow 4\tau$.

These final states have several taus, and most of them have missing energy. After the tau decays, all channels present a large amount of missing energy. The criteria used to eliminate almost all remaining $f\bar{f}\gamma$ events and most of the 4-fermion events were the following:

- the missing energy had to be greater than $0.3\cdot\sqrt{s}$;
- the energy in a cone of half-angle of 30° around the beam axis was required to be less than 40% of the total visible energy;
- the number of charged (neutral) particles had to be less than 8 (10);
- the energy of the most energetic lepton had to be between 2 and 70 GeV;
- at least one lepton should have a polar angle between 40° and 140°;
- there should be no other charged particle in a cone with a half-angle of 6° around at least one lepton;
- y_{32} and y_{43}, computed with the `DURHAM` algorithm, (Fig. 4–b) had to be greater than $2 \cdot 10^{-3}$ and $4 \cdot 10^{-4}$ respectively;
- in a four-jet topology a minimum angle of 20° between any pair of jets was required.

4.3.4 $\widetilde{\nu}_\tau$ search

An analysis searching for 2e2τ final states produced in the direct decay of $\widetilde{\nu}_\tau\bar{\widetilde{\nu}}_\tau$ was performed. Compared to the selection described in 4.3.3, the most important change was the suppression of the criterion on the missing energy, and the introduction of the requirement of having at least one well identified electron:

- the energy in a cone of 30° around the beam axis was required to be less than 50% of the total visible energy;
- the number of charged (neutral) particles had to be less than 7 (10);
- there should be at least one electron;
- the energy of the most energetic lepton had to be between 25 and 80 GeV;
- at least one lepton should have a polar angle between 40° and 140°;
- there should be no other charged particle in a cone of half-angle of 6° around at least one lepton;
- y_{32} (Fig. 4–c), computed with the `DURHAM` algorithm, had to be greater than $2 \cdot 10^{-3}$;
- in a four-jet topology, a minimum angle of 20° between any pair of jets was required.

This selection removed $f\bar{f}\gamma$ background and most of the 4-fermion events.

4.3.5 Stop search

In stop pair-production, each of the stops decays into a charm quark and a neutralino. The subsequent R_p-violating decay via the λ_{133} coupling of the neutralino into leptons, the final state: $2\tau + 2\ell + \not{E} + 2j$, ℓ =e or τ.

After the preselection described in Section 4.3.1, the criteria used to select the final states of the stop pair indirect decay were:

- the missing energy greater than $0.3\cdot\sqrt{s}$;
- the charged and neutral particle multiplicities below 25 and 20 respectively;

- the polar angle of at least one lepton between 40° and 140°;
- the energy of the most energetic identified lepton between 5 and 50 GeV;
- no other charged particle in a cone of half-angle of 6° around at least one lepton;
- at least one well identified electron (Fig. 4–d);
- the y_{32} and y_{54} values constrained to be less than 0.016 and 10^{-3} respectively;
- in the four-jet configuration, at least one jet with less than three charged particles.

4.4 Multi-jet $\bar{U}\bar{D}\bar{D}$ channels

For all $\bar{U}\bar{D}\bar{D}$ channels the main SM backgrounds come from four-fermion processes except for the low neutralino mass channel where the hadronic Z decay is the dominant background. The following $\bar{U}\bar{D}\bar{D}$ analyses were based on neural network techniques since the optimisation of the signal selection over the four-fermion background was performed on topological variables, such as jet resolution parameters, which are extensively correlated.

4.4.1 Preselection

The multi-jet $\bar{U}\bar{D}\bar{D}$ signals have final states with a large hadronic activity, independent of the produced sparticles. Therefore a general hadronic preselection was performed with the aim of a high efficiency for the signal (especially for the gaugino analysis) and at the same time a good rejection of low particle multiplicity hadronic background events:

- the number of charged particles had to be greater than 15;
- the total energy was required to be greater than $0.6{\cdot}\sqrt{s}$;
- the energy associated to charged particles was required to be greater than $0.3{\cdot}\sqrt{s}$;
- the effective centre-of-mass energy [5] had to be greater than 150 GeV;
- the discriminating variable $d_\alpha = \alpha_{\min} \cdot E_{\min} - 0.5 \cdot \beta_{\min} \cdot E_{\max}/E_{\min}$ (where the 0.5 energy factor is in GeV) had to be greater than –10 GeV.rad [6];
- the minimum jet invariant mass had to be greater than 500 MeV/c^2 when forcing the event into four jets;
- the $\ln(y_{32})$ had to be greater than –6.9;
- the $\ln(y_{43})$ had to be greater than –8.

After the hadronic preselection, the main remaining background events were the four-fermion events and the $q\bar{q}\gamma$ events with hard gluon radiation. We observed 3844 events in the data with 3869 ± 4 events expected from background processes for the year 2000 (4180 events in the data to be compared to 4096 ± 7 events in the simulation for the year 1999). Examples of the distributions of several event variables at the hadronic preselection level are shown in Figure 5.

The efficiencies for the $\bar{U}\bar{D}\bar{D}$ signals varied from 60% to 99% depending on the simulated masses and ΔM. This preselection (sometimes with slight modifications, described in the following) was used for all the $\bar{U}\bar{D}\bar{D}$ analyses.

These requirements had to be slightly modified to be better optimised for slepton searches. The discriminating variable d_α was not used in the preselection, and the effective centre-of-mass energy was required to be above $0.6{\cdot}\sqrt{s}$, because a tighter cut was set on y_{43} and a cut on y_{54} was applied.

Additional criteria to the basic hadronic preselection have been applied before the optimal neural network selection:

[5] the effective centre-of-mass energy is the centre-of-mass energy after the emission of one or more photons from the initial state.

[6] $\alpha_{\min}$ is the minimum angle between two jets, $\beta_{\min}$ is the minimum angle between the most energetic jet and any other, $E_{\min}$ ($E_{\max}$) is the minimum (maximum) jet energy from the four-jet topology of the event.

- the charged particle multiplicity had to be greater than 16;
- the total energy was required to be greater than $0.6 \cdot \sqrt{s}$;
- the energy of charged particles was required to be greater than $0.3 \cdot \sqrt{s}$;
- the $\ln(y_{43})$ had to be greater than –7;
- the $\ln(y_{54})$ had to be greater than –8;
- the thrust had to be lower than 0.94;
- the maximum di-jet mass in a four-jet configuration had to be greater than 10 GeV/c^2.

This selection was applied for the $\bar{\mathrm{U}}\bar{\mathrm{D}}\bar{\mathrm{D}}$ sleptons ans squark analyses. After this selection the remaining number of events for all energies was 4245 for the data and 4378 $\pm$ 8 for the expected background from SM processes.
The distributions of the variables $\ln(y_{54})$ and $\ln(y_{65})$ at this stage of the preselection level are shown in Figure 6.

4.4.2 Neutralino search

The analysis described here was mainly designed to search for neutralino direct decays; it was also efficient in the search for chargino direct decays. The six-jet analyses were based on three different neural networks for the optimization of the background and signal discrimination. The neural network method used has been presented in Section 4.2.3.

Events with low gaugino mass have a large boost and look like di-jet events. On the contrary, events with heavy gauginos are almost spherical with six well separated jets. Therefore, we distinguished 3 mass windows to increase the sensitivity of each signal configuration:

- low mass window N1: $10 \leq m_{\tilde{\chi}} \leq 45$ GeV/c^2;
- medium mass window N2: $45 < m_{\tilde{\chi}} \leq 75$ GeV/c^2;
- high mass window N3: $m_{\tilde{\chi}} > 75$ GeV/c^2.

A mass reconstruction was performed using a method depending on the mass window. For the N1 analysis, the events were forced into two jets and the average of the two-jet masses was computed. For the other analyses, the events were forced into six jets and criteria on di-jet angles were applied to choose the optimum three-jet combinations corresponding to the decays of two neutralinos with the same mass. The minimum and maximum angles between the jets belonging to the same three-jet cluster (same neutralino) had to be in the intervals $[20°, 80°]$ and $[50°, 165°]$ for the medium mass window N2 ($[40°, 110°]$ and $[100°, 175°]$ for the high mass window N3). If more than one combination was selected, the combination with the minimum difference between the two energies of the three-jet clusters was chosen to compute the neutralino mass.

Three neural networks were used, one for each mass window, with the following variables as inputs:

- the thrust;
- $\mathrm{dist_{WW}} = \sqrt{\frac{(M_1 - M_2)^2}{\sigma_-^2} + \frac{(M_1 + M_2 - 2M_W)^2}{\sigma_+^2}}$, where M_1 and M_2 are the di-jet masses of the jet combination which minimized this variable (after forcing the event into 4 jets); we took $M_W = 80.4$ GeV/c^2 for the W mass, $\sigma_- = 9.5$ GeV/c^2 and $\sigma_+ = 4.8$ GeV/c^2 for the mass resolutions of the difference and the sum of the reconstructed di-jet masses respectively; this variable is peaked at 0 for WW events, allowing a good discrimination against this background;

- the energy of the least energetic jet multiplied by the minimum di-jet angle in four and five-jet configurations;
- the difference between the energies of the two combinations of three jets, after the mass reconstruction;
- the reconstructed neutralino mass;
- $y_{n\ n-1}$ with n=3 to 10.

It was observed that the modelling of the gluon emission was unable to describe the event distributions of $y_{n\ n-1}$ correctly for n greater than 5. To take into account this imperfect description, corrections were applied to the background distributions of the $y_{n\ n-1}$ variables (for n between 6 and 10) [30].

4.4.3 Chargino search

To take into account the effect of the mass difference between chargino and neutralino, ΔM, on the topology of the event, the ten-jet analysis was divided into two windows:

- low ΔM window C1: $5 \leq \Delta M \leq 10$ GeV/c^2;
- high ΔM window C2: $\Delta M > 10$ GeV/c^2.

Two neural networks were trained with the following discriminating variables as inputs:

- the thrust;
- the variable $\mathrm{dist_{WW}}$ described above;
- the energy of the least energetic jet multiplied by the minimum di-jet angle in four and five-jet configurations;
- $y_{n\ n-1}$ with n=3 to 10 (for n=6 to 10, the corrected $y_{n\ n-1}$ were used); for the C1 analysis, the variables y_{87}, y_{98} and $y_{10\,9}$ were not used.

4.4.4 Slepton search

Three mass windows were defined to take into account the mass difference, ΔM, between the sfermion and the neutralino considered as the LSP:

- low ΔM window 1: $5 \leq \Delta M \leq 10$ GeV/c^2 with $m_{\tilde{\chi}^0} > 55$ GeV/c^2;
- high ΔM window 2: $\Delta M > 10$ GeV/c^2 with $m_{\tilde{\chi}^0} > 55$ GeV/c^2;
- low neutralino mass window 3: $m_{\tilde{\chi}^0} \leq 55$ GeV/c^2.

Different selection criteria on the momentum of the tagged leptons were applied depending on the mass window.

Electron and muon momentum selection

In addition to the high rejection power of the topological jet variables, lepton identification has been used since two opposite sign leptons of the same flavour are produced in the final state (see Table 2). Therefore, an electron and positron, or two muons with opposite sign were required, with thresholds on the momentum which depended on ΔM, in order to discriminate the selectron or the smuon pair-production signal from the SM background:

- the momentum of the less energetic tagged lepton (electron or muon) had to be lower than 30 GeV/c (window 1), 70 GeV/c (windows 2 and 3);
- the momentum of the more energetic tagged electron had to be in the intervals [2,40] GeV/c (window 1), [10,70] GeV/c (window 2) and [10,90] GeV/c (window 3);
- the momentum of the more energetic tagged muon had to be in the intervals [2,40] GeV/c (window 1), [30,70] GeV/c (window 2) and [30,90] GeV/c (window 3).

Neural network signal selection optimisation

The following variables have been used as inputs to the neural networks:

- the clustering variables y_{43}, y_{54}, y_{65}, computed with the `CAMBRIDGE` algorithm;
- the minimum di-jet mass in the four, five and six-jet configurations;
- the energy of the least energetic jet · minimum di-jet angle in four and five-jet configurations;
- the thrust (only for window 3);
- the energy of the most energetic electromagnetic cluster (only for window 3).

The training was performed on signal samples of selectrons and smuons at centre-of-mass energies of 200 and 206 GeV for each analysis, and with the same statistics for two samples of the most important expected SM backgrounds (two and four-fermion events separately).

4.4.5 Squark search

Searches for stop and sbottom were performed in the case of indirect decays. The eight quarks event topology depends strongly on ΔM, the mass difference between the squark and the $\widetilde{\chi}_1^0$. The same mass windows as those defined for slepton analysis (Section 4.4.4) were used. After the preselection and before training the neural networks, additional criteria were applied to select high jet multiplicity events:

- the total multiplicity had to be lower than 40;
- the effective centre-of-mass energy had to be greater than $0.7 \cdot \sqrt{s}$;
- the total electromagnetic energy had to be lower than 20 GeV (window 3 only);
- the $\ln(y_{43})$ had to be greater than -6;
- the $\ln(y_{54})$ had to be greater than -6.5;
- the momentum of the less energetic tagged electron had to be lower than 16 GeV/c (windows 1 and 2), 20 GeV/c (window 3);
- the momentum of the most energetic tagged electron had to be lower than 40 GeV/c;
- the energy of the most energetic electromagnetic cluster had to be lower than 40 GeV (window 3 only).

Sbottom decays produce b–quarks in the final state which may be identified with the impact parameter information provided by the micro-vertex detector. The event tagging obtained with the DELPHI algorithm for tagging events containing a b–quark [31] was therefore added as a sequential cut for the sbottom analysis.

The same input variables as in the selectron and smuon searches (Section 4.4.4) were used in the neural network, except for the low ΔM analysis, where the energy of the most energetic electromagnetic cluster was suppressed.

5 Results and limits

In this section, the number of selected and expected events after the final event selection, and the signal efficiencies obtained for each channel under study are presented. The results are in agreement with the SM expectation. Together with the signal efficiencies they were used to exclude at 95% CL possible regions of the MSSM parameter space. Unless otherwise stated, the limits were derived using the results from the centre-of-mass energies between 192 and 208 GeV.

As already mentioned, to obtain the most conservative constraints on the MSSM parameter values from $LL\bar{E}$ searches, only the analyses performed considering the λ_{133}

coupling as the dominant one were used: in fact, if a different λ_{ijk} coupling is dominant, the exclusions would be at least as large as those from a dominating λ_{133} coupling.

After a presentation of the methods applied to derive limits, the efficiencies and the number of selected events are given for each channel, as well as the derived limits.

5.1 Limit computation

Limits on gaugino masses

An upper limit to the number of signal events, N_{95}, at 95% CL, was calculated according to the monochannel Bayesian method [32] from the number of events remaining in the data and those expected in the SM, summed over all centre-of-mass energies from 192 to 208 GeV.

The gaugino pair-production was considered for different values of tanβ (from 0.5 to 30), m_0 (between 90 GeV/c^2 and 500 GeV/c^2), μ (between –200 GeV/c^2 and 200 GeV/c^2) and M_2 (between 5 and 400 GeV/c^2); for a given set of tanβ and m_0 values the (μ, M_2) point was excluded at 95% CL if the expected number of signal, N_{exp} at this point was greater than N_{95}. The computations of N_{exp} were slightly different for $LL\bar{E}$ and $\bar{U}\bar{D}\bar{D}$ searches, as detailed below.

To obtain the limits on the gaugino masses with a good precision, special studies were performed to scan the regions of the parameter space from which the limits were determined: the steps in M_2 and μ were of 0.25 GeV/c^2 and 1 GeV/c^2, respectively.

Limits on sfermion masses

For all the sfermion searches the limits at 95% CL were derived using the modified frequentist likelihood ratio method [33]. Expected exclusion limits were obtained with the same algorithm where the number of observed events was set to the number of expected background events (absence of signal). To extract the mass limits, a branching ratio of 100% was assumed for the R_p-conserving decay of the sfermion into a neutralino and a fermion. The MSSM values chosen to present the exclusion plots were tanβ = 1.5 and μ = –200 GeV/c^2.

The statistical errors on the efficiencies, which were between ±1% and ±3%, and on the expected background were used in the limit computation, for gauginos and sfermions. The systematic uncertainties on the signal selection efficiencies were negligeable compared to statistical errors in the $LL\bar{E}$ analyses. In the case of $\bar{U}\bar{D}\bar{D}$ analyses, the systematic uncertainties on the signal efficiences were larger. Indeed, the hard gluon radiation in the parton shower of the Monte Carlo $\bar{U}\bar{D}\bar{D}$ signal simulation is not implemented. Therefore this generates systematically events with background-like y_{mn} distributions. This is the reason why the $\bar{U}\bar{D}\bar{D}$ results of the present search are conservative.

5.2 Gaugino searches

5.2.1 $LL\bar{E}$ scenario

Efficiencies and selected events

The efficiency of the selection described in Section 4.3.2 was computed from simulated samples at different points of the MSSM parameter space. In order to benefit from the high centre-of-mass energies and luminosities, all $e^+e^- \rightarrow \widetilde{\chi}_i^0\widetilde{\chi}_j^0$ and $e^+e^- \rightarrow \widetilde{\chi}_1^+\widetilde{\chi}_1^-$

processes which contribute significantly have been simulated, at each MSSM point of this study. Then a global event selection efficiency was determined for each point. The efficiencies lay between 11% and 38%.

At each selection step of the gaugino analysis, good agreement between the number of observed and expected background events was obtained, and no excess was observed in the data; at the end, 24 candidates remained in the data from 192 to 208 GeV, compared to 23.7 ± 0.6 expected from SM background processes (see Table 3), mainly from W^+W^- events and the rest from other four-fermion processes.

Limits

The number of expected events corresponding to gaugino pair-production at each point of the explored MSSM parameter space was obtained by:

$$N_{exp} = \epsilon_{200} \cdot \sum_{E_{cm}=192}^{E_{cm}=202} \mathcal{L}_{E_{cm}} \cdot \sigma_{\chi\chi} + \epsilon_{206} \cdot \sum_{E_{cm}=203}^{E_{cm}=208} \mathcal{L}_{E_{cm}} \cdot \sigma_{\chi\chi}$$

where $\sigma_{\chi\chi} = \sum_{i,j=1}^{4} \sigma(e^+e^- \rightarrow \widetilde{\chi}_i^0 \widetilde{\chi}_j^0) + \sigma(e^+e^- \rightarrow \widetilde{\chi}_1^+ \widetilde{\chi}_1^-)$, $\mathcal{L}_{E_{cm}}$ is the integrated luminosity collected at the centre-of-mass energy E_{cm}, and ϵ_{200} and ϵ_{206} are the global efficiencies determined as explained above at 200 and 206 GeV respectively. All points which satisfied $N_{exp} > N_{95}$ were excluded at 95% CL, and the corresponding excluded area in (μ, M_2) planes obtained with the present searches are presented in Figure 7, for m_0 = 90, 500 GeV/c^2 and tanβ =1.5, 30.

For each tanβ, the highest value of the mass of the lightest neutralino which can be excluded has been determined in the (μ, M_2) plane for several m_0 values from 90 to 500 GeV/c^2; the most conservative mass limit was obtained for high m_0 values. The corresponding limit on neutralino mass as a function of tanβ is shown in Figure 8.
The same procedure has been applied to determine the most conservative lower limit on the chargino mass. The result is less dependent on tanβ, and almost reaches the kinematic limit for any value of tanβ. The lower limit obtained on the neutralino mass is 39.5 GeV/c^2, and the one on the chargino mass is 103.0 GeV/c^2.

5.2.2 $\bar{U}\bar{D}\bar{D}$ scenario

Efficiencies and selected events

At the end of the analysis procedure to search for gauginos described in Sections 4.4.2 and 4.4.3, no significant excess of events was seen in the data with respect to the SM expectations. Figure 9 shows the number of expected events from the SM and the number of observed events as a function of the average signal efficiency obtained with all simulated masses for the N3 and C2 analyses after a step-by-step cut on the neural network output.

For neutralino pair-production, the efficiencies were typically around 30–60% at the values of the optimized neural network outputs, depending on the simulated masses. For chargino pair-production, the signal efficiencies were between 10% and 70%. The expected and observed numbers of events for both analyses are reported in Table 3 for each mass window.

Limits

The signal efficiency for any values of the $\widetilde{\chi}_1^0$ and $\widetilde{\chi}^{\pm}$ masses was interpolated using an efficiency grid determined with signal samples produced with the full DELPHI detector simulation. The number of expected events N_{exp} has been computed separatly for neutralino and chargino pair productions.

$$N_{exp} = \epsilon_{200} \cdot \sum_{E_{cm}=192}^{E_{cm}=202} \mathcal{L}_{E_{cm}} \cdot \sigma_{\chi\chi} + \epsilon_{206} \cdot \sum_{E_{cm}=203}^{E_{cm}=208} \mathcal{L}_{E_{cm}} \cdot \sigma_{\chi\chi}$$

where $\sigma_{\chi\chi} = \sigma(e^+e^- \to \widetilde{\chi}_1^0\widetilde{\chi}_1^0)$ or $\sigma(e^+e^- \to \widetilde{\chi}_1^+\widetilde{\chi}_1^-)$, and ϵ_{200} and ϵ_{206} are taken from the efficiency grids.

Using the six-jet and the ten-jet analysis results, an exclusion contours in the (μ, M_2) plane at 95% CL were derived for different values of m_0 (90 and 300 GeV/c^2) and tanβ (1.5 and 30), as shown in Figure 10. In the exclusion plots the main contribution comes from the study of the chargino indirect decays with the ten-jet analysis, due to the high cross-section. The six-jet analysis becomes crucial in the exclusion plot for low tanβ, low m_0 and negative μ. The lower limits on the mass of the lightest neutralino and chargino are obtained from the scan on tanβ from 0.5 to 30. The lower limit on the neutralino mass of 38.0 GeV/c^2 is obtained for tanβ = 1 and m_0 = 500 GeV/c^2 (Figure 11). The chargino is mainly excluded up to the kinematic limit at 102.5 GeV/c^2.

5.3 Slepton searches

5.3.1 LL$\bar{E}$ scenario

Efficiencies and selected events

The efficiencies of the slepton analysis described in Section 4.3.3 were between 18% and 38% for the sneutrino indirect decay channel, depending only on the neutralino mass. The efficiencies were higher for the final states obtained in indirect decay of charged slepton pairs, due to the presence of two additional leptons. They ranged from $\sim$ 20% ($m_{\widetilde{\chi}^0}$ = 15 GeV/c^2) to 43% for stau pairs; they were of the same order but up to $\sim$ 5% higher for selectron pairs, and ranged from $\sim$ 25% ($m_{\widetilde{\chi}^0}$ = 15 GeV/c^2) to 64% for smuon pairs. For the direct decay of $\widetilde{\nu}_e$, the analysis efficiencies lay in the range 27–36%, depending on the sneutrino mass.

At the end of the selection, 11 events remained in the data compared to 8.1 $\pm$ 0.3 expected from the SM processes (Table 3). The background was mainly composed of four–fermion events, in particular from W pair-production.

The efficiencies of the $\widetilde{\nu}_\tau\widetilde{\nu}_\tau$ direct decay analysis (see Section 4.3.4) varied with the $\tilde{\nu}_\tau$ mass and ranged from 45% to 51%. At the end of the selection, 6 candidates were obtained for 6.3 $\pm$ 0.4 expected (see Table 3).

Limits

To derive limits on slepton masses, the results of the search described above were combined with those obtained with data at $\sqrt{s}$ = 189 GeV [3].

For charged slepton indirect decay, the areas excluded in the $m_{\widetilde{\chi}^0}$ versus $m_{\tilde{\ell}_R}$ planes are plotted in Figure 12.

As was explained in Section 2.3, a pair of selectrons can be produced in the t-channel via neutralino exchange. With the MSSM parameters fixed to derive limits, the $\tilde{e}^+\tilde{e}^-$ cross-section is higher than the $\tilde{\mu}^+\tilde{\mu}^-$ and $\tilde{\tau}^+\tilde{\tau}^-$ ones. So, though the analysis efficiencies for the smuon pair-production were higher, the excluded area in case of the selectron pair search is the largest; the smallest is obtained for the $\tilde{\tau}^+\tilde{\tau}^-$ production. For $\Delta M \geq 5$ GeV/c^2, the limits on the slepton mass are 94 GeV/c^2, 87 GeV/c^2 and 86 GeV/c^2 for the $\tilde{e}$, $\tilde{\mu}$ and $\tilde{\tau}$, respectively, and become 95 GeV/c^2, 90 GeV/c^2 and 90 GeV/c^2 if the neutralino mass limit is taken into account.

The results of the search for the indirect decay of the $\tilde{\nu}$ were used to exclude areas in the $m_{\widetilde{\chi}^0}$ versus $m_{\tilde{\nu}}$ planes, as shown in Figure 13. These exclusion areas are also

valid for all the λ_{ijk} couplings. As already mentioned in Section 2.3, the $\widetilde{\nu}_{\rm e}\widetilde{\bar{\nu}}_{\rm e}$ cross-section can be enhanced compared to the $\widetilde{\nu}_{\mu}\widetilde{\bar{\nu}}_{\mu}$ and $\widetilde{\nu}_{\tau}\widetilde{\bar{\nu}}_{\tau}$ cross-sections if production via a chargino exchange is possible and the excluded area depends on the chargino mass. For ΔM $\geq$ 5 GeV/c^2, the limit on the $\widetilde{\nu}_{\mu}$ and $\widetilde{\nu}_{\tau}$ mass is 82 GeV/c^2, and is 85 GeV/c^2 if the limit on the neutralino mass is taken into account. These limits are 96 and 98 GeV/c^2 respectively for $\widetilde{\nu}_{\rm e}$.

The results of the searches for 4τ and $2e2\tau$ final states, from sneutrino pair direct decays, were combined to obtain lower limits on the sneutrino mass. The results from the 4τ search were used to derive limits on $\widetilde{\nu}_{\rm e}$ and on $\widetilde{\nu}_{\mu}$, those from the $2e2\tau$ to derive limits on $\widetilde{\nu}_{\tau}$. The limits obtained are respectively 96 GeV/c^2, 83 GeV/c^2 and 91 GeV/c^2.

5.3.2 $\bar{\rm U}\bar{\rm D}\bar{\rm D}$ scenario

Efficiencies and selected events

No significant excess has been observed in the output signal node distributions for any analyses. The signal output distributions for the selectrons and smuons analyses are shown in Figure 14 for the medium ΔM analyses. The signal efficiency of the slepton analyses described in Section 4.4.4 was evaluated at each of the simulated points for the two centre-of-mass energies (200 and 206 GeV). Efficiencies for the signal (selectron and smuon) were in the range from 5–40%, for small mass differences and small neutralino mass, and increased up to 60% for medium ΔM analyses. The 5% efficiency was obtained for the ΔM = 5 GeV and for a neutralino mass of 45 GeV. This efficiency increased rapidly with ΔM and with the neutralino mass.

No excess of data with respect to the SM expectations was observed for the selectron and smuon analyses; the numbers of events observed and expected from background contributions are shown in Table 3. The remaining background comes mainly from four-fermion processes.

Limits

From the selectron and smuon pair-production searches exclusion domains have been computed in the $m_{\tilde{\chi}^0}$ versus $m_{\tilde{\ell}_R}$ plane (Figures 15). The M_2 value was fixed for each neutralino mass. For ΔM$\geq$ 5 GeV/c^2, the lower limit on the right-handed selectron mass was 92 GeV/c^2, and the lower limit obtained for the right-handed smuon was 85 GeV/c^2.

5.4 Squark searches

5.4.1 LL$\bar{\rm E}$ scenario

Efficiencies and selected events

The selection efficiencies of the analysis described in 4.3.5 varied with the stop mass and with the mass difference between the stop and the lightest neutralino. They lay around 30% for most of cases, and around 18–20% for low neutralino masses.

After the selection procedure, 35 events remained with 35.4 $\pm$ 0.6 expected from background contributions, mostly coming from W^+W^- production.

Limits

From the study of the stop indirect decay, a lower limit on the stop pair-production cross-section was derived as a function of the stop and neutralino masses. Considering

two cases of stop mixing (no mixing and mixing angle = 56°), the exclusion limit was derived in the $m_{\tilde{\chi}_1^0}$ versus $m_{\tilde{t}}$ plane, as shown in Figure 16. With no mixing, the lower bound on the stop mass is 88 GeV/c^2, valid for $\Delta M > 5$ GeV/c^2. If the mixing angle is 56°, the lower bound on the stop mass is 81 GeV/c^2, for $\Delta M > 5$ GeV/c^2, and becomes 87 GeV/c^2, taking into account the lower limit on the mass of the lightest neutralino.

5.4.2 $\bar{U}\bar{D}\bar{D}$ scenario

Efficiencies and selected events

The final selection of candidate events was based on the signal output values of the neural networks for the stop and for the sbottom. The cut on the neural network variable has been relaxed for sbottom due to the effect of the b-tagging selection. The signal outputs of the neural network for the multi-jet stop and sbottom analyses (window 3) are shown in Figure 17. The signal efficiencies of the neural network analyses described in 4.4.5 were evaluated at each of the evenly distributed simulated points in the plane of stop (sbottom) and neutralino masses. Efficiencies for the signal after the final selection were in the range from 10–20%, for small or large mass differences between squark and neutralino, up to around 50% for medium mass differences.

The numbers of events observed and expected from SM processes are shown in Table 3.

Limits

The resulting exclusion contours for stop and sbottom can be seen in Figures 18 and 19. The lower limit on the mass of the left-handed stop, assuming the neutralino mass limit of 38 GeV/c^2, is 87 GeV/c^2 for $\Delta M \geq 5$ GeV/c^2. The lower limit on the stop mass with the mixing angle = 56° was 77 GeV/c^2 under the same assumptions. The lower limit obtained for the left-handed sbottom assuming a neutralino mass limit of 38 GeV/c^2, was 78 GeV/c^2 for $\Delta M \geq 5$ GeV/c^2. The sbottom pair-production cross-section in the case of the mixing angle corresponding to maximum decoupling from the Z boson (68° for sbottom) was too low to cover a significant region of the mass plane by the excluded cross-section of the sbottom analyses.

6 Summary

A large number of different searches for supersymmetric particles with the assumption of R_p violation via $\lambda_{ijk}L_iL_j\bar{E}_k$ or $\lambda''_{ijk}\bar{U}_i\bar{D}_j\bar{D}_k$ terms have been performed on the data recorded in 1999 and 2000 by the DELPHI experiment, at centre-of-mass energies between 192 and 208 GeV. No significant excess has been observed in any of the channels. Limits on the pair-production of sparticles have been derived. These limits were converted into limits on sparticle masses and excluded regions in the MSSM parameter space. Mass limits are summarized in Table 4, together with the assumptions under which these limits are valid.

Acknowledgements

We are greatly indebted to our technical collaborators, to the members of the CERN-SL Division for the excellent performance of the LEP collider, and to the funding agencies for their support in building and operating the DELPHI detector.
We acknowledge in particular the support of
Austrian Federal Ministry of Education, Science and Culture, GZ 616.364/2-III/2a/98,
FNRS–FWO, Flanders Institute to encourage scientific and technological research in the industry (IWT), Belgium,
FINEP, CNPq, CAPES, FUJB and FAPERJ, Brazil,
Czech Ministry of Industry and Trade, GA CR 202/99/1362,
Commission of the European Communities (DG XII),
Direction des Sciences de la Matière, CEA, France,
Bundesministerium für Bildung, Wissenschaft, Forschung und Technologie, Germany,
General Secretariat for Research and Technology, Greece,
National Science Foundation (NWO) and Foundation for Research on Matter (FOM), The Netherlands,
Norwegian Research Council,
State Committee for Scientific Research, Poland, SPUB-M/CERN/PO3/DZ296/2000, SPUB-M/CERN/PO3/DZ297/2000, 2P03B 104 19 and 2P03B 69 23(2002-2004)
FCT - Fundação para a Ciência e Tecnologia, Portugal,
Vedecka grantova agentura MS SR, Slovakia, Nr. 95/5195/134,
Ministry of Science and Technology of the Republic of Slovenia,
CICYT, Spain, AEN99-0950 and AEN99-0761,
The Swedish Natural Science Research Council,
Particle Physics and Astronomy Research Council, UK,
Department of Energy, USA, DE-FG02-01ER41155.
EEC RTN contract HPRN-CT-00292-2002.

References

[1] For reviews, see e.g. H.P. Nilles, *Phys. Rep.***110** (1984) 1;
H.E. Haber and G.L. Kane, *Phys. Rep.* **117** (1985) 75.
[2] P. Fayet, *Phys. Lett.* **B69** (1977) 489;
G. Farrar and P. Fayet, *Phys. Lett.* **B76** (1978) 575.
[3] P. Abreu *et al.* [DELPHI Collaboration], *Eur. Phys. J.* **C13** (2000) 591;
P. Abreu *et al.* [DELPHI Collaboration], *Phys. Lett.* **B487** (2000) 36.
[4] P. Abreu *et al.* [DELPHI Collaboration], *Phys. Lett.* **B500** (2001) 22.
[5] A. Heister *et al.* [ALEPH Collaboration], *Eur. Phys. J.* **C31** (2003) 1;
P. Achard *et al.* [L3 Collaboration], *Phys. Lett.* **B524** (2002) 65;
G. Abbiendi *et al.* [OPAL Collaboration], *Eur. Phys. J.* **C33** (2004) 149.
[6] S. Weinberg, *Phys. Rev.* **D26** (1982) 287.
[7] V. Barger, G.F. Giudice and T. Han, *Phys. Rev.* **D40** (1989) 2987.
[8] B.C. Allanach, A. Dedes and H.K. Dreiner, *Phys. Rev.* **D60** (1999) 075014.
[9] H. Dreiner and G.G. Ross, *Nucl. Phys.* **B365** (1991) 597.
[10] S. Dawson, *Nucl. Phys.* **B261** (1985) 297.
[11] J. Abdallah *et al.* [DELPHI Collaboration], CERN-EP-2003-007.

[12] J. Abdallah *et al.* [DELPHI Collaboration], *Eur. Phys. J.* **C27** (2003) 153;
P. Abreu *et al.* [DELPHI Collaboration], *Phys. Lett.* **B485** (2000) 95.
[13] J. Abdallah *et al.* [DELPHI Collaboration], *Eur. Phys. J.* **C28** (2003) 15.
[14] J. Ellis and S. Rudaz, *Phys. Lett.* **B128** (1983) 248.
[15] A. Bartl et al., *Zeit. Phys.* **C76** (1997) 549.
[16] M. Drees, "An introduction to supersymmetry" Lectures given at Inauguration Conference of the Asia Pacific Center for Theoretical Physics (APCTP), Seoul, Korea, 4-19 Jun 1996; hep-ph/9611409.
[17] M. Drees and S.P. Martin, "Implications of SUSY model building," hep-ph/9504324.
[18] M. Drees and K. Hikasa, *Phys. Lett.* **B252** (1990) 127.
[19] P. Aarnio *et al.*, *Nucl. Instr. Meth.* **303** (1991) 233;
P. Abreu *et al.*, *Nucl. Instr. Meth.* **378** (1996) 57.
[20] F.A. Berends, P.H. Daverveldt, R. Kleiss, *Computer Phys. Comm.* **40** (1986) 271, 285 and 309.
[21] S. Jadach, W. Placzek, B.F.L. Ward, *Phys. Lett.* **B390** (1997) 298.
[22] S. Jadach, Z. Was, *Computer Phys. Comm.* **79** (1994) 503.
[23] T. Sjostrand, *Computer Phys. Comm.* **82** (1994) 74.
[24] F.A. Berends, R. Kleiss, R. Pittau, *Computer Phys. Comm.* **85** (1995) 437.
[25] J. Fujimoto *et al.*, *Computer Phys. Comm.* **100** (1997) 128.
[26] S. Katsanevas, P. Morawitz, *Computer Phys. Comm.* **112** (1998) 227;
N. Ghodbane, *Proceedings of the Worldwide Study on Physics and Experiments with Future Linear e^+e^- Colliders*, Sitges, Barcelona, Spain, 28 April – 5 May 1999.
[27] S. Catani et al., *Phys. Lett.* **B269** (1991) 432.
[28] Yu.L. Dokshitzer, G.D. Leder, S. Moretti, B.R. Webber, *J. High Energy Phys.* 8 (1997) 1.
[29] S. Bentvelsen and I. Meyer, *Eur. Phys. J.* **C4** (1998) 623.
[30] V. Poireau, DAPNIA/SPP-01-01-T, PhD thesis (2001) in French.
[31] P. Abreu et al., *Eur. Phys. J.* **C10** (1999) 415.
[32] R.M. Barnett et al., Particle Data Group, *Phys. Rev.* **D54** (1996) 1.
[33] A. Read *et al, 1st Workshop on Confidence Limits*, CERN 2000-005, 81-103.

$\sqrt{s}$ (GeV)	192	196	200	202	<204.9>	<206.6>	<206.6>
$\mathcal{L}$ (pb^{-1})	25.1	76.0	83.3	42.5	73.7	85.4	51.8

Table 1: Data collected by DELPHI in 1999 and 2000: the integrated luminosities correspond to the data actually used in the present analyses after the run selection. The last column refers to the integrated luminosity collected with one sector of the TPC off.

LL$\bar{\text{E}}$: multi–lepton topologies

analysis name	final states	direct decays of	indirect decays of
gaugino	2τ + nℓ + mj + $\not{E}$ (n≥2) (m≥0)	$\widetilde{\chi}_1^0\widetilde{\chi}_1^0$	$\widetilde{\chi}_1^+\widetilde{\chi}_1^-$ $\widetilde{\chi}_i^0\widetilde{\chi}_j^0$
slepton	$2\tau + 2\ell + \not{E}$ + pℓ (p = 0 or 2)		$\tilde{\nu}\bar{\tilde{\nu}}$, $\widetilde{\ell}^+\widetilde{\ell}^-$
	$\tau\tau\tau\tau$	$\widetilde{\nu}_{\text{e}}\widetilde{\bar{\nu}}_{\text{e}}$	
sneutrino tau	ee$\tau\tau$	$\widetilde{\nu}_\tau\widetilde{\bar{\nu}}_\tau$	
squark	$2\tau + 2\ell + \not{E} + 2j$		$\widetilde{\text{q}}\widetilde{\bar{\text{q}}}$

$\bar{\text{U}}\bar{\text{D}}\bar{\text{D}}$: multi–jet topologies

analysis name	final states	direct decays of	indirect decays of
neutralino	$6j$	$\widetilde{\chi}_1^0\widetilde{\chi}_1^0$, $\widetilde{\chi}_1^+\widetilde{\chi}_1^-$	
chargino	$10j$		$\widetilde{\chi}_1^+\widetilde{\chi}_1^-$
slepton	$6j + 2\ell$		$\widetilde{\ell}^+\widetilde{\ell}^-$
squark	$8j$		$\widetilde{\text{q}}\widetilde{\bar{\text{q}}}$

Table 2: The multi-lepton and multi-jet visible final states which correspond to the analyses described in this paper, when one LL$\bar{\text{E}}$ or $\bar{\text{U}}\bar{\text{D}}\bar{\text{D}}$ term is dominant. The corresponding pairs of produced sparticles that may have given rise to them are indicated. For the LL$\bar{\text{E}}$ cases, only topologies produced with decays via λ_{133} are considered (see text), and for the $\bar{\text{U}}\bar{\text{D}}\bar{\text{D}}$ cases, ℓ = e or μ.

$LL\bar{E}$: multi–lepton topologies

Analysis name	192–202 GeV observed	192–202 GeV expected		203–208 GeV observed	203–208 GeV expected	
gaugino	15	13.4	$\pm$ 0.4	9	10.3	$\pm$ 0.4
slepton	4	4.2	$\pm$ 0.2	7	3.9	$\pm$ 0.2
sneutrino τ	3	3.5	$\pm$ 0.3	3	2.8	$\pm$ 0.2
squark	19	19.9	$\pm$ 0.5	16	15.5	$\pm$ 0.4

$\bar{U}\bar{D}\bar{D}$: multi–jet topologies

Analysis name	Mass windows (GeV/c^2)	192–202 GeV observed	192–202 GeV expected		203–208 GeV observed	203–208 GeV expected	
neutralino	$15 \leq m_{\tilde{\chi}} \leq 45$	134	126.0	$\pm$ 13.0	121	119.3	$\pm$ 8.8
	$45 < m_{\tilde{\chi}} \leq 75$	192	172.5	$\pm$ 8.2	167	164.7	$\pm$ 5.7
	$75 < m_{\tilde{\chi}}$	97	103.3	$\pm$ 3.6	82	91.7	$\pm$ 2.3
chargino	$\Delta M \leq 10$	187	181.1	$\pm$ 5.9	156	171.7	$\pm$ 5.2
	$\Delta M > 10$	22	25.6	$\pm$ 1.1	20	23.5	$\pm$ 1.0
slepton	$m_{\tilde{\chi}} > 55$, $\Delta M \leq 10$	9	5.6	$\pm$ 0.2	1	6.2	$\pm$ 0.2
($\tilde{e}$)	$m_{\tilde{\chi}} > 55$, $\Delta M > 10$	1	2.0	$\pm$ 0.1	5	2.3	$\pm$ 0.1
	$15 \leq m_{\tilde{\chi}} \leq 55$	1	1.6	$\pm$ 0.1	0	1.8	$\pm$ 0.1
slepton	$m_{\tilde{\chi}} > 55$, $\Delta M \leq 10$	7	5.7	$\pm$ 0.2	5	6.4	$\pm$ 0.2
($\tilde{\mu}$)	$m_{\tilde{\chi}} > 55$, $\Delta M > 10$	4	3.3	$\pm$ 0.2	1	3.5	$\pm$ 0.2
	$15 \leq m_{\tilde{\chi}} \leq 55$	2	2.0	$\pm$ 0.1	1	2.3	$\pm$ 0.1
squark	$m_{\tilde{\chi}} > 55$, $\Delta M \leq 10$	42	39.4	$\pm$ 0.6	38	40.4	$\pm$ 0.6
($\tilde{t}$)	$m_{\tilde{\chi}} > 55$, $\Delta M > 10$	13	10.1	$\pm$ 0.3	8	9.5	$\pm$ 0.3
	$15 \leq m_{\tilde{\chi}} \leq 55$	30	26.3	$\pm$ 0.5	25	25.2	$\pm$ 0.5
squark	$m_{\tilde{\chi}} > 55$, $\Delta M \leq 10$	10	11.9	$\pm$ 0.4	13	12.0	$\pm$ 0.4
($\tilde{b}$)	$m_{\tilde{\chi}} > 55$, $\Delta M > 10$	4	5.4	$\pm$ 0.2	7	4.8	$\pm$ 0.2
	$15 \leq m_{\tilde{\chi}} \leq 55$	6	4.6	$\pm$ 0.2	8	4.2	$\pm$ 0.2

Table 3: Observed and expected numbers of events for all $LL\bar{E}$ and $\bar{U}\bar{D}\bar{D}$ analyses. Although not explicitely written, ΔM is always greater than 5 GeV/c^2.

SUSY particle	Comments about validity conditions	Mass limit (GeV/c^2) LL$\bar{\text{E}}$	$\bar{\text{U}}\bar{\text{D}}\bar{\text{D}}$
$\widetilde{\chi}_1^0$	Validity conditions for gauginos: $90 < m_0 < 500$ GeV/c^2, $0.7 < \tan\beta < 30$,	39.5	38.0
$\widetilde{\chi}_1^+$	$-200 < \mu < 200$ GeV/c^2 and $0 < M_2 < 400$ GeV/c^2	103.0	102.5
	Validity conditions for sfermions: $\mu = -200$ GeV/c^2 and $\tan\beta = 1.5$, BR($\tilde{f} \rightarrow$ f' $\widetilde{\chi}_1^0$)=1, $\Delta M > 5$ GeV/c^2		
$\widetilde{e}_R$	$\widetilde{\chi}_1^0$ mass limit not used	94	92
	$\widetilde{\chi}_1^0$ mass limit used	95	92
$\widetilde{\mu}_R$	$\widetilde{\chi}_1^0$ mass limit not used	87	85
	$\widetilde{\chi}_1^0$ mass limit used	90	87
$\widetilde{\tau}_R$	$\widetilde{\chi}_1^0$ mass limit not used	86	–
	$\widetilde{\chi}_1^0$ mass limit used	90	–
$\widetilde{\nu}_e$	$\widetilde{\chi}_1^0$ mass limit not used	96	–
	$\widetilde{\chi}_1^0$ mass limit used	98	–
	direct decay only	96	×
$\widetilde{\nu}_\mu$	$\widetilde{\chi}_1^0$ mass limit not used	82	–
	$\widetilde{\chi}_1^0$ mass limit used	85	–
	direct decay only	83	×
$\widetilde{\nu}_\tau$	$\widetilde{\chi}_1^0$ mass limit not used	82	–
	$\widetilde{\chi}_1^0$ mass limit used	85	–
	direct decay only	91	×
$\tilde{t}$	$\widetilde{\chi}_1^0$ mass limit not used, no mixing	88	81
	$\widetilde{\chi}_1^0$ mass limit used, no mixing	92	87
	$\widetilde{\chi}_1^0$ mass limit not used, minimal mixing	81	67
	$\widetilde{\chi}_1^0$ mass limit used, minimal mixing	87	77
$\tilde{b}$	$\widetilde{\chi}_1^0$ mass limit not used, no mixing	–	78
	$\widetilde{\chi}_1^0$ mass limit used, no mixing	–	78

Table 4: Sparticle mass limits at 95% CL from the DELPHI R_p violation pair-production searches of supersymmetric particles; ×: the decay channel is not possible; –: the decay channel is not covered. These results are valid if $m_{\widetilde{\chi}_1^0} \geq 15$ GeV/c^2, except for the $\tilde{\nu}$ mass limits derived from the $\tilde{\nu}$ direct decay which does not depend on $m_{\widetilde{\chi}_1^0}$.

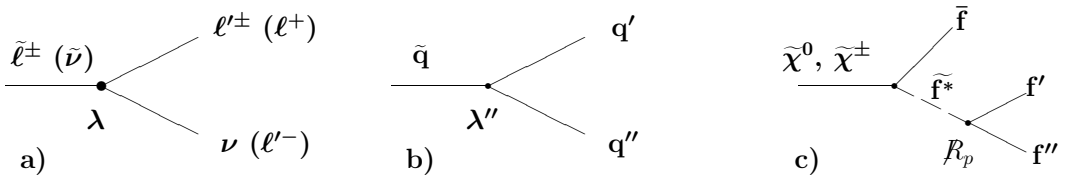

Figure 1: Diagrams of sparticle direct decays. a: slepton direct decay via $LL\bar{E}$ term; b: squark direct decay via $\bar{U}\bar{D}\bar{D}$ term; c: neutralino/chargino direct decay via any R_p-violating trilinear term.

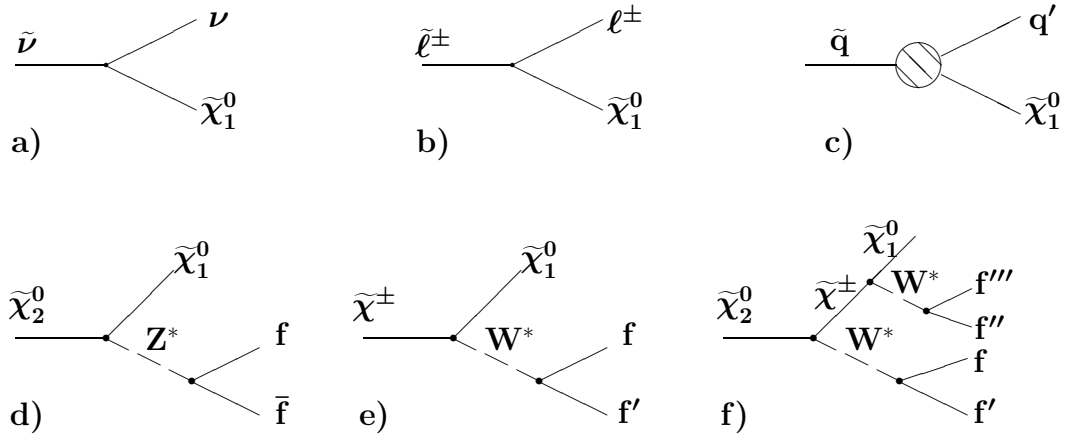

Figure 2: Diagrams of sparticle R_p-conserving decays. To get the whole chain of the sparticle indirect decay, the LSP (lightest neutralino) has to undergo a direct R_p-violating decay. a, b: slepton decays into a lepton and the lightest neutralino; c: squark decay into a quark and the lightest neutralino, the hatched disk means decay beyond tree level for the stop case; d, e, f: examples of gaugino decays.

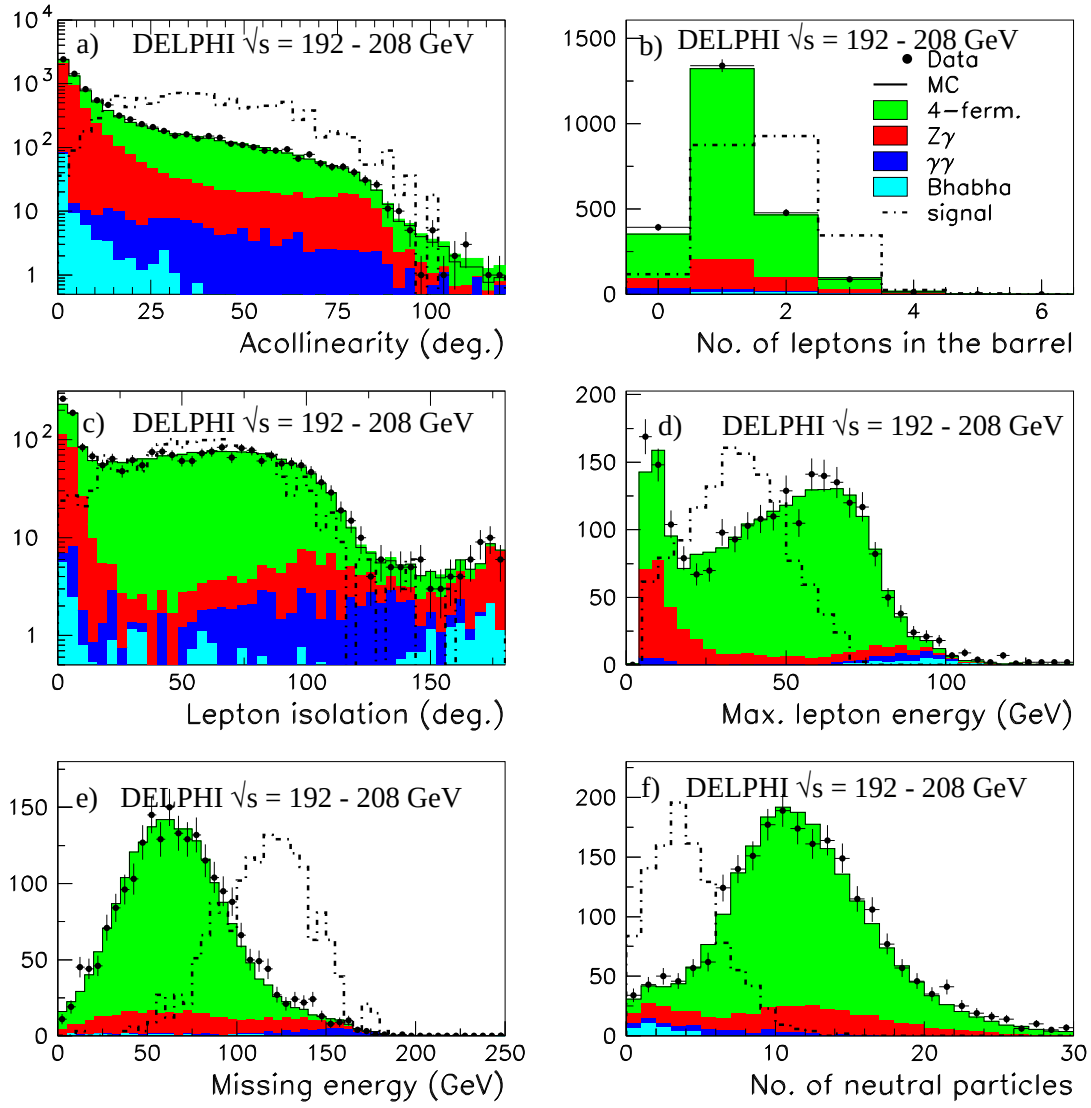

Figure 3: LL$\bar{\text{E}}$: sparticle pair search in multi-lepton channels – Event variable (see text) distributions before the criteria applied on the acollinearity (preselection) (a) and after (b–f) the preselection. The simulated signal corresponds to $\widetilde{\chi}^0_1\widetilde{\chi}^0_1$ production, with $m_{\chi^0_1} = 90$ GeV/c^2 (the normalisation is arbitrary).

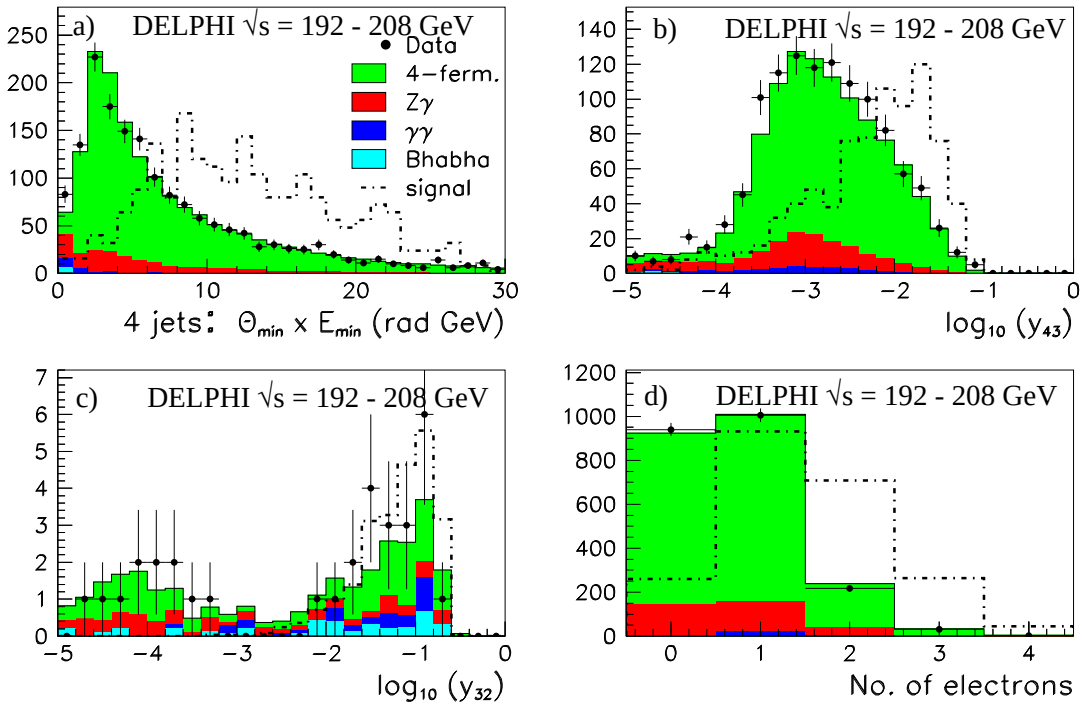

Figure 4: LL$\bar{\mathrm{E}}$: sparticle pair search in multi-lepton channels – Distributions of variables used in the four analyses, as described in the text: a) gaugino, b) slepton, c) sneutrino tau, d) squark. The simulated signals correspond to production of a) $\widetilde{\chi}_2^0\widetilde{\chi}_1^0$ and $\widetilde{\chi}_1^+\widetilde{\chi}_1^-$ ($\mathrm{m}_{\widetilde{\chi}_1^0} = 50$ GeV/c^2, $\mathrm{m}_{\widetilde{\chi}_2^0} = 85$ GeV/c^2, $\mathrm{m}_{\widetilde{\chi}_1^\pm} = 95$ GeV/c^2), b) $\widetilde{\nu}_\mathrm{e}\bar{\widetilde{\nu}}_\mathrm{e}$ ($\mathrm{m}_{\widetilde{\nu}_\mathrm{e}} = 100$ GeV/c^2), c) $\widetilde{\nu}_\tau\bar{\widetilde{\nu}}_\tau$ ($\mathrm{m}_{\widetilde{\nu}_\tau} = 95$ GeV/c^2), d) $\widetilde{\mathrm{t}}\bar{\widetilde{\mathrm{t}}}$ ($\mathrm{m}_{\widetilde{\mathrm{t}}} = 95$ GeV/c^2) (the signal normalisation is arbitrary).

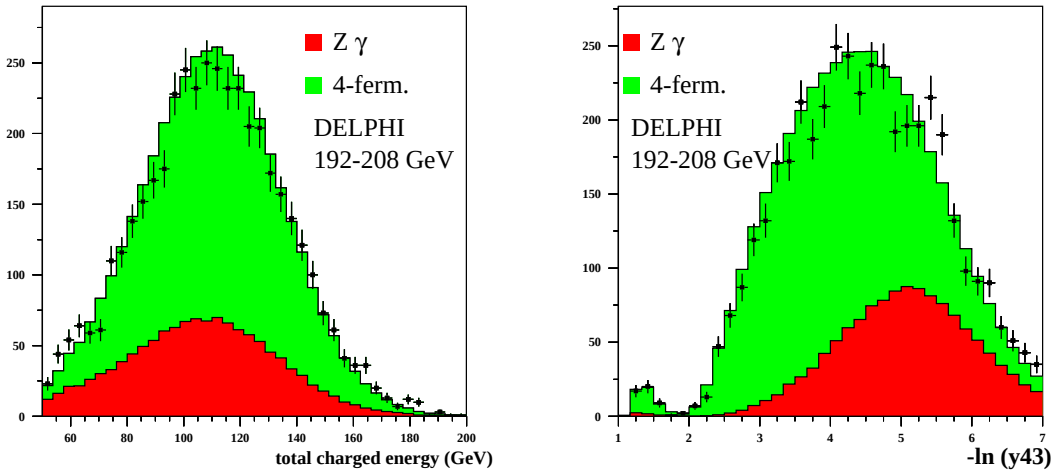

Figure 5: $\bar{U}\bar{D}\bar{D}$: the total energy associated to charged particles (left) and -ln(y_{43}) (right) distributions in the multi-jet slepton analyses at the hadronic preselection level.

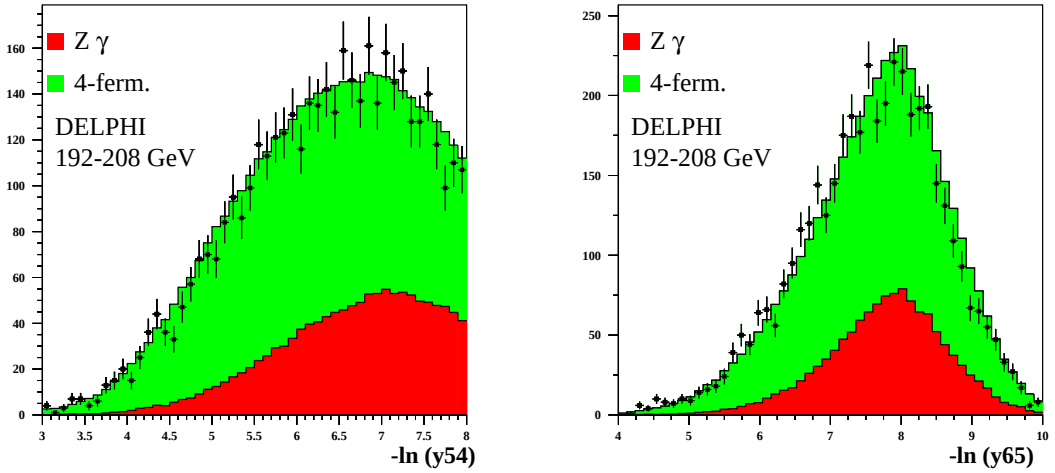

Figure 6: $\bar{U}\bar{D}\bar{D}$: the -ln(y_{54}) (left) and -ln(y_{65}) (right) distributions in the multi-jet sfermion analyses at preselection level.

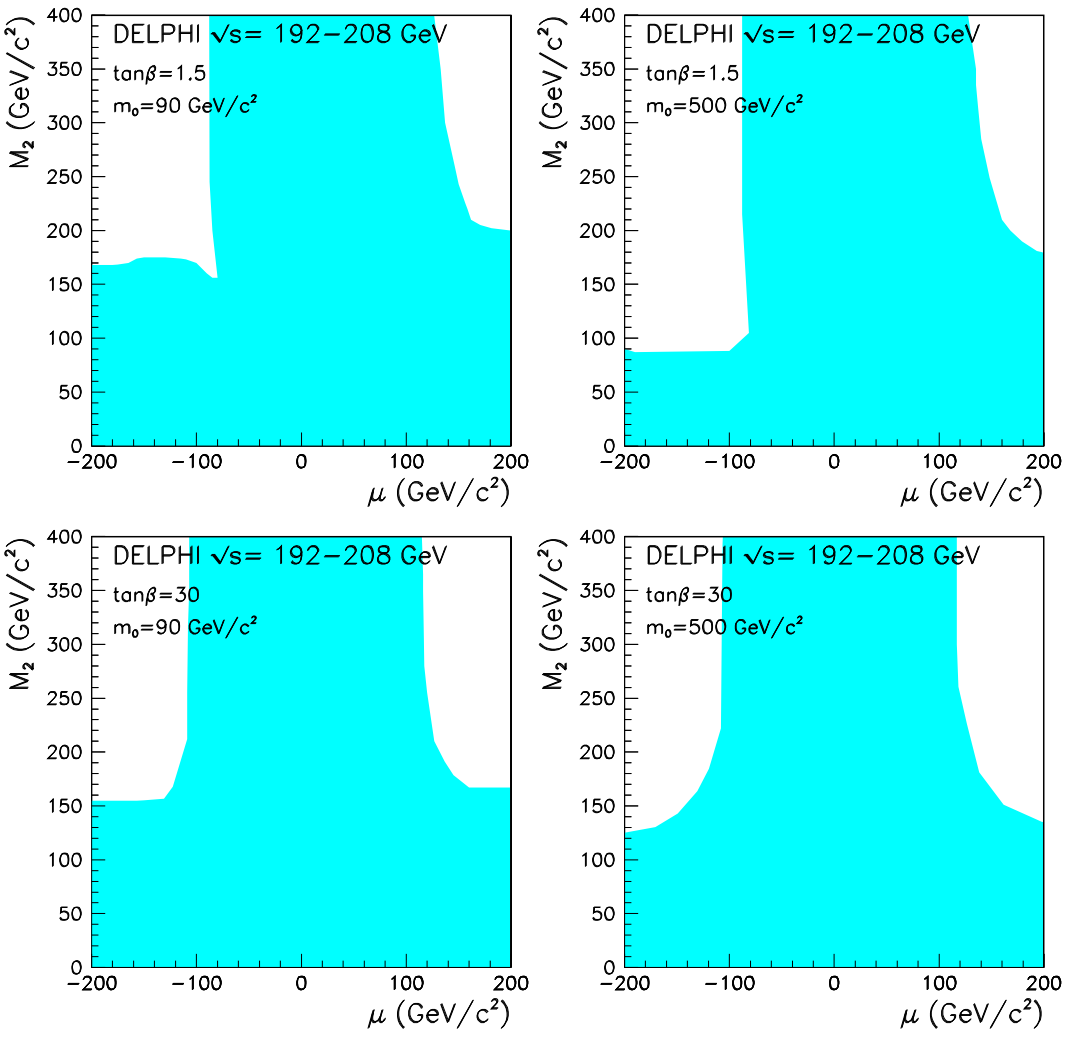

Figure 7: LL$\bar{\text{E}}$: regions in μ, M_2 parameter space excluded at 95% CL by the neutralino and chargino searches for two values of tanβ and two values of m_0.

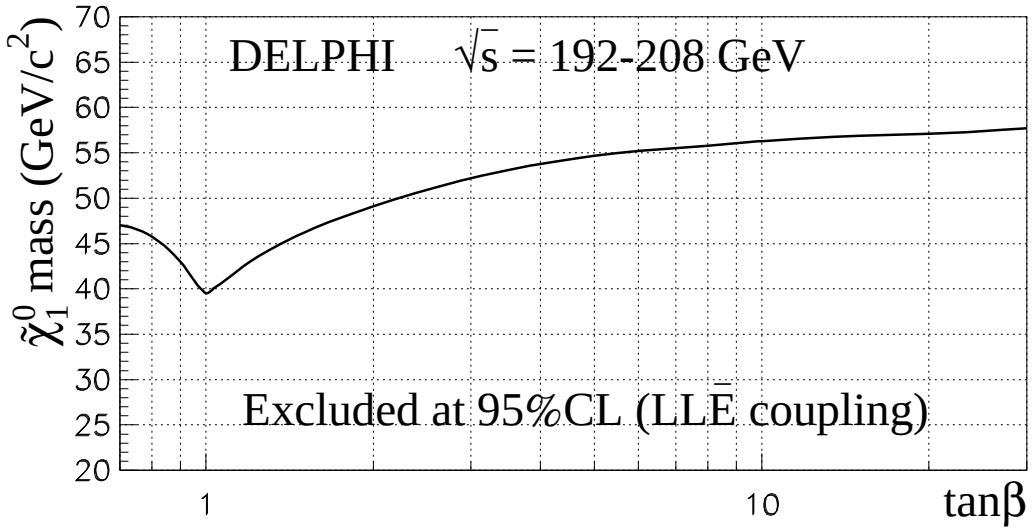

Figure 8: LL$\bar{\text{E}}$: excluded lightest neutralino mass as a function of tanβ at 95% CL. This limit is independent of the choice of the generation indices i,j,k of the λ_{ijk} coupling and is for values of m_0 between 90 and 500 GeV/c^2.

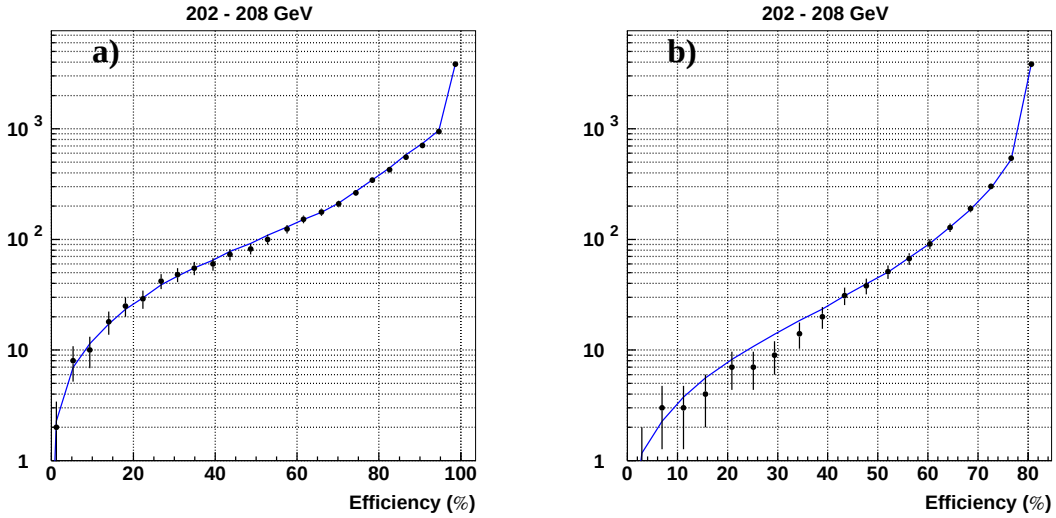

Figure 9: $\bar{\text{U}}\bar{\text{D}}\bar{\text{D}}$: number of expected events (continuous line) and data events (black dots) versus average signal efficiency for the high neutralino mass search N3 (plot a) and for the large ΔM chargino search C2 (plot b) for centre-of-mass energies between 202 and 208 GeV.

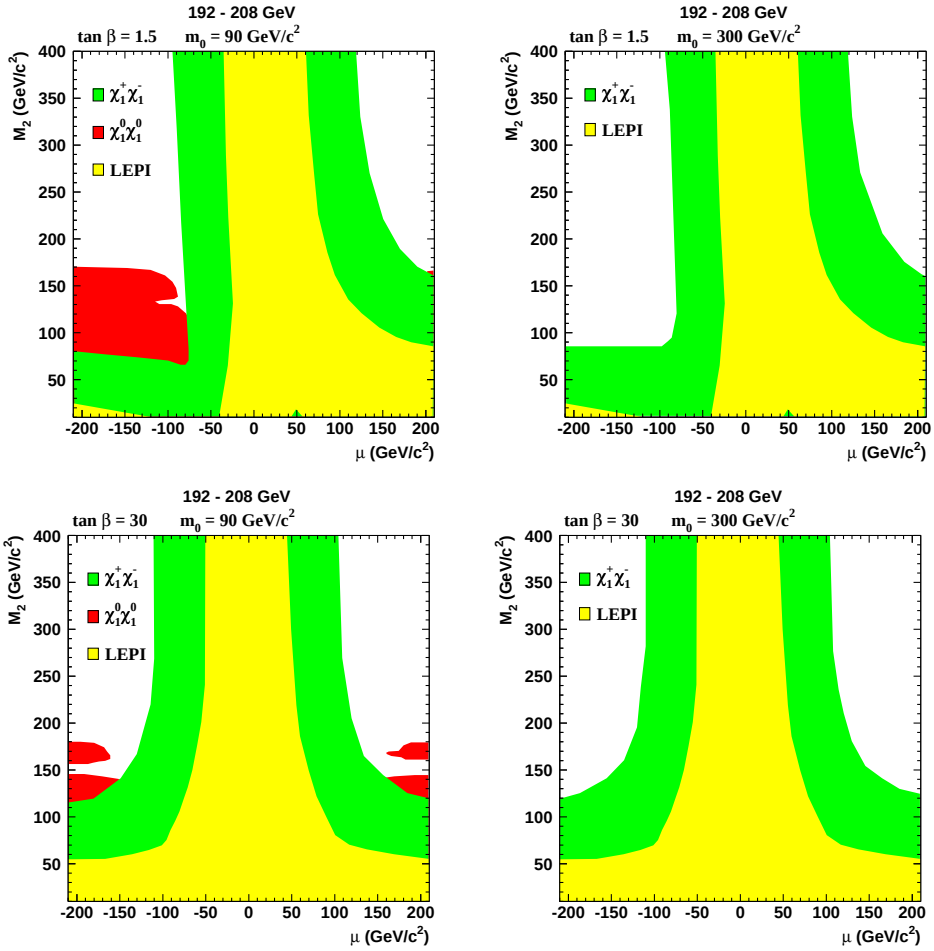

Figure 10: $\bar{\mathrm{U}}\bar{\mathrm{D}}\bar{\mathrm{D}}$: regions in μ, M_2 parameter space excluded at 95% CL by the neutralino and chargino searches for two values of tanβ and two values of m_0.

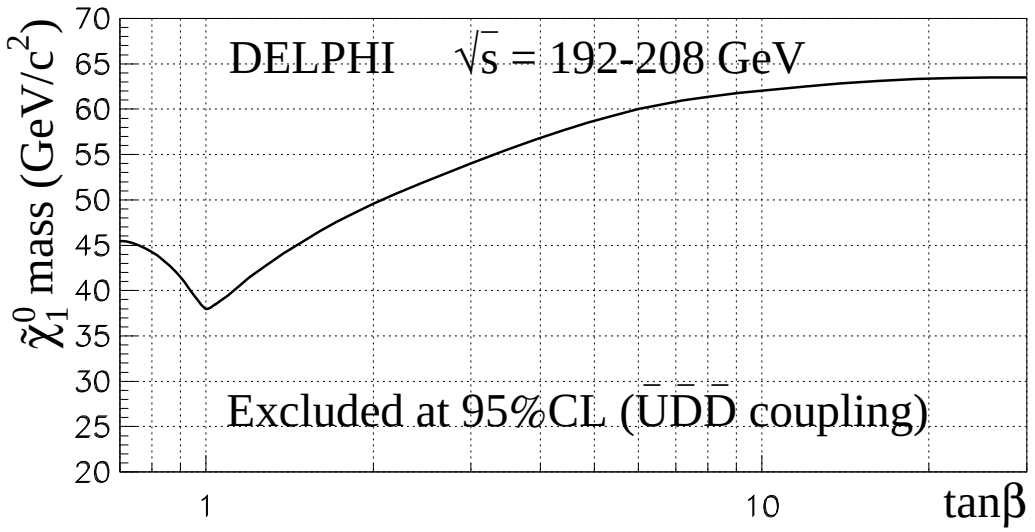

Figure 11: $\bar{U}\bar{D}\bar{D}$: lightest neutralino mass excluded at 95% CL as a function of tanβ. This limit was obtained for m_0= 500 GeV/c^2.

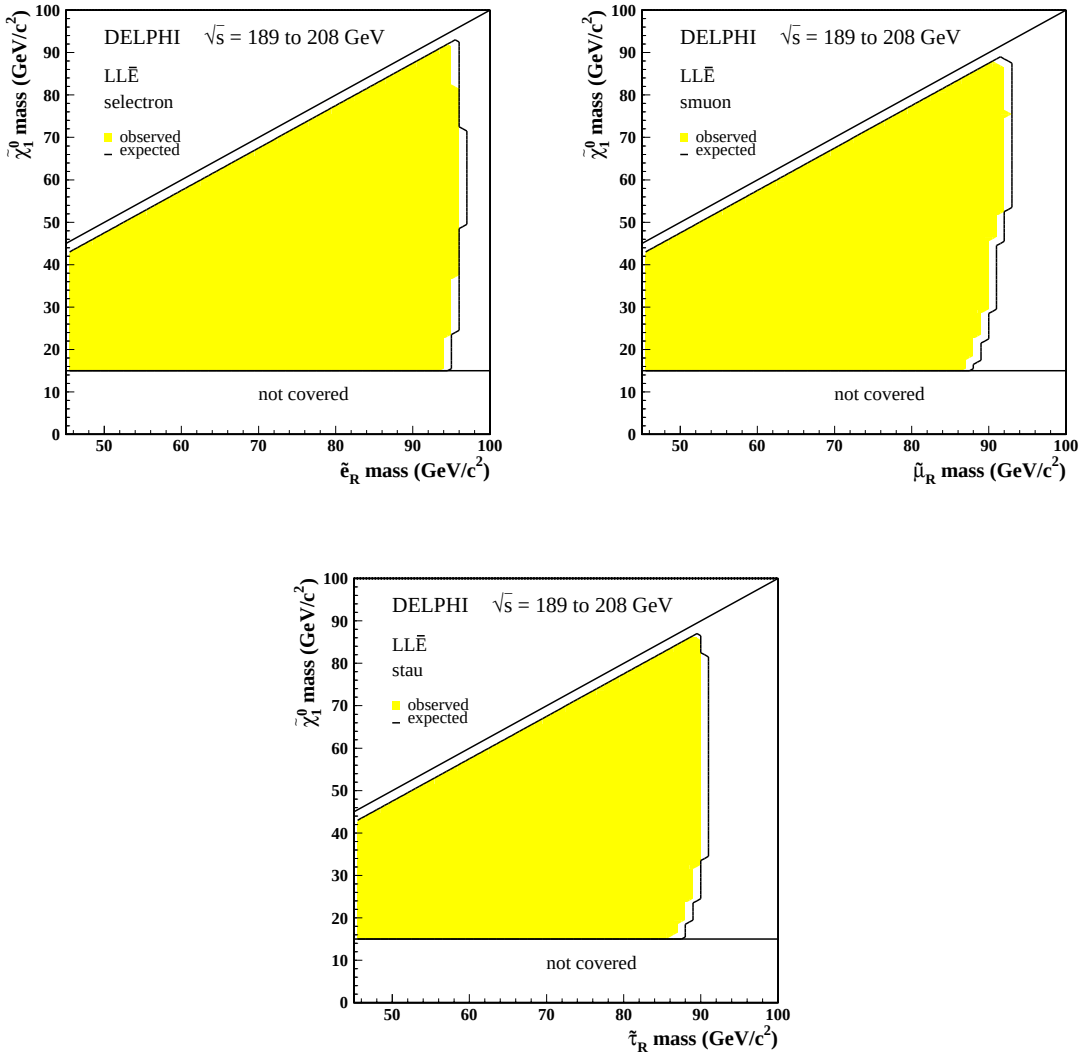

Figure 12: LL$\bar{\text{E}}$: excluded regions at 95% CL in the $m_{\tilde{\chi}^0}$ versus $m_{\tilde{\ell}_R}$ planes for $\tilde{\ell}_R$ pair-production, with BR($\tilde{\ell}_R \to \widetilde{\chi}_1^0\ \ell$) = 100%, and neutralino decay into leptons. The plots show the exclusion (filled area) for selectron, smuon and stau. The black contour is the corresponding expected exclusion at 95% CL.

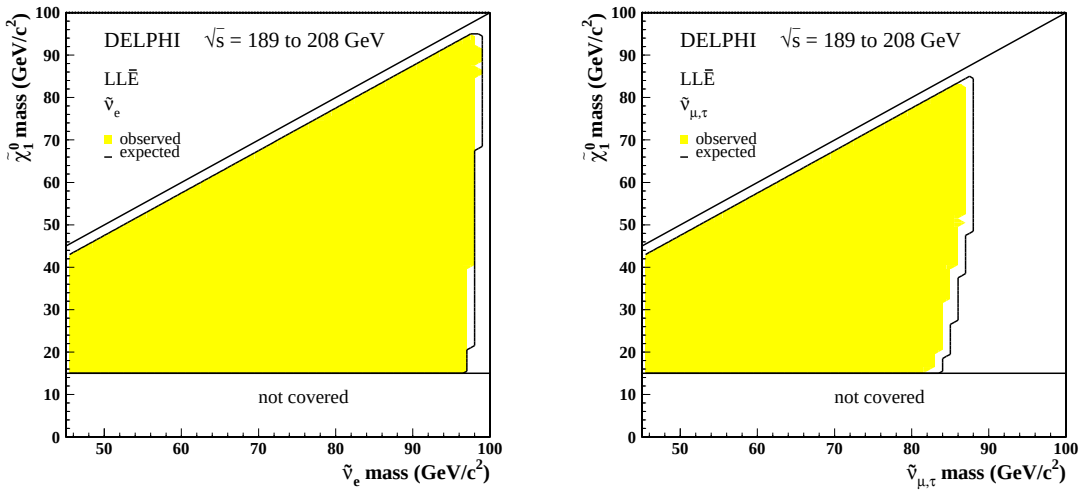

Figure 13: LL$\bar{\text{E}}$: excluded regions at 95% CL in the $m_{\tilde{\chi}^0}$ versus $m_{\tilde{\nu}}$ planes for $\widetilde{\nu}_e$ (left) and $\widetilde{\nu}_\mu$,$\widetilde{\nu}_\tau$ (right) pair-production, with BR($\tilde{\nu} \to \widetilde{\chi}^0_1\ \nu$) = 100%, and neutralino decay into leptons. The black contour is the corresponding expected exclusion at 95% CL.

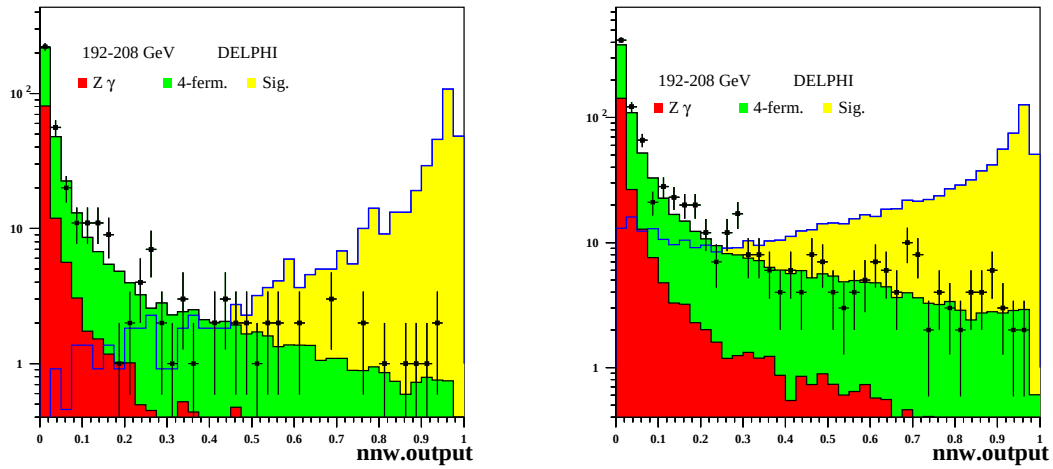

Figure 14: $\bar{\mathrm{U}}\bar{\mathrm{D}}\bar{\mathrm{D}}$: the neural network signal output distributions for the selectron (left) and smuon (right) window 2 analyses. The cuts on the neural network output variable were chosen for the final selection at 0.83 (selectrons) and 0.92 (smuons).

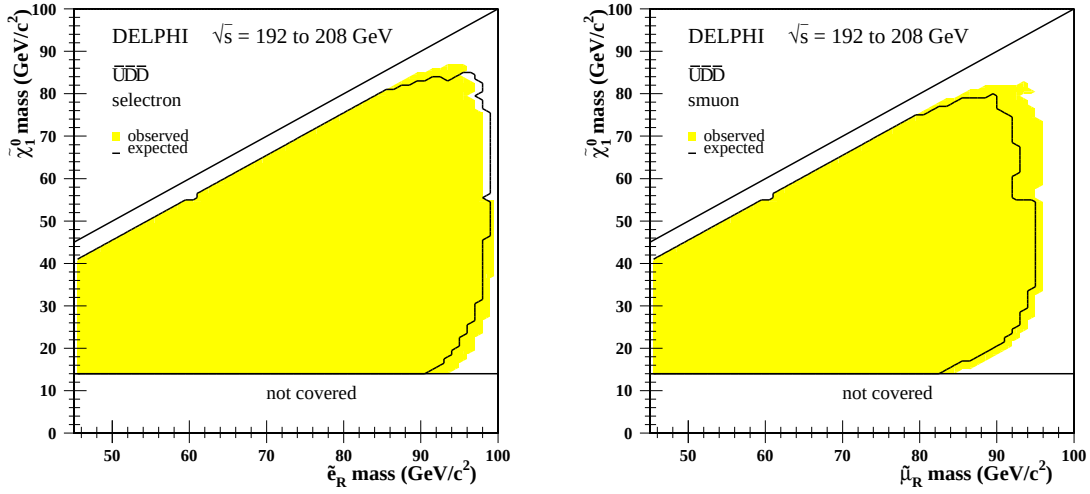

Figure 15: $\bar{\mathrm{U}}\bar{\mathrm{D}}\bar{\mathrm{D}}$: excluded domains at 95% CL in the $\mathrm{m}_{\tilde{\chi}_1^0}$ versus $\mathrm{m}_{\tilde{\ell}}$ planes for selectron (left) and for smuon (right) pair-production with $\mathrm{BR}(\tilde{\ell}_R \rightarrow \tilde{\chi}_1^0\ \ell) = 100\%$ and neutralino decay into jets (filled area). The superimposed contours show the expected exclusion at 95% CL.

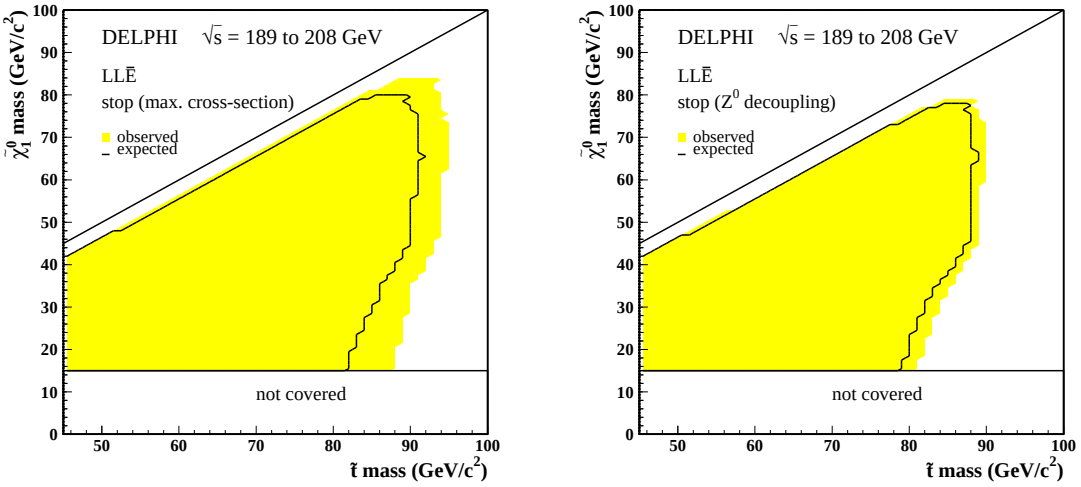

Figure 16: LL$\bar{\text{E}}$: exclusion domains at 95% CL in the $m_{\tilde{\chi}^0}$ versus $m_{\tilde{t}}$ plane for the stop pair-production, with BR($\tilde{t} \rightarrow c\tilde{\chi}_1^0$) = 100% and neutralino decay into leptons. The plots show the exclusion (filled area) for the lightest stop for no mixing (left) and for the mixing leading to the maximal decoupling to the Z boson (right). The black contour is the corresponding expected exclusion at 95% CL.

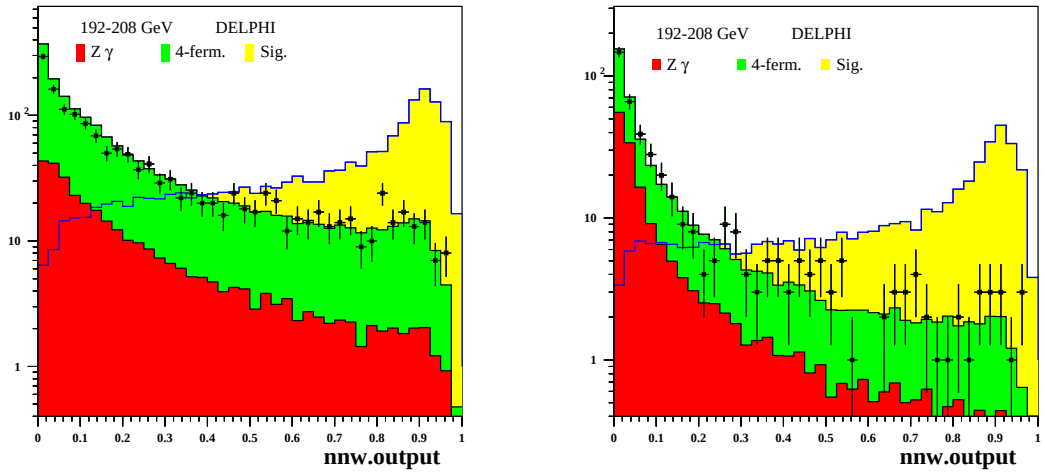

Figure 17: $\bar{\text{U}}\bar{\text{D}}\bar{\text{D}}$: the neural network signal output distributions for the multi-jet stop (left) and sbottom (right) window 3 analyses. The cuts on the neural network output variable were chosen for the final selection at 0.86 and 0.75 for stop and sbottom respectively.

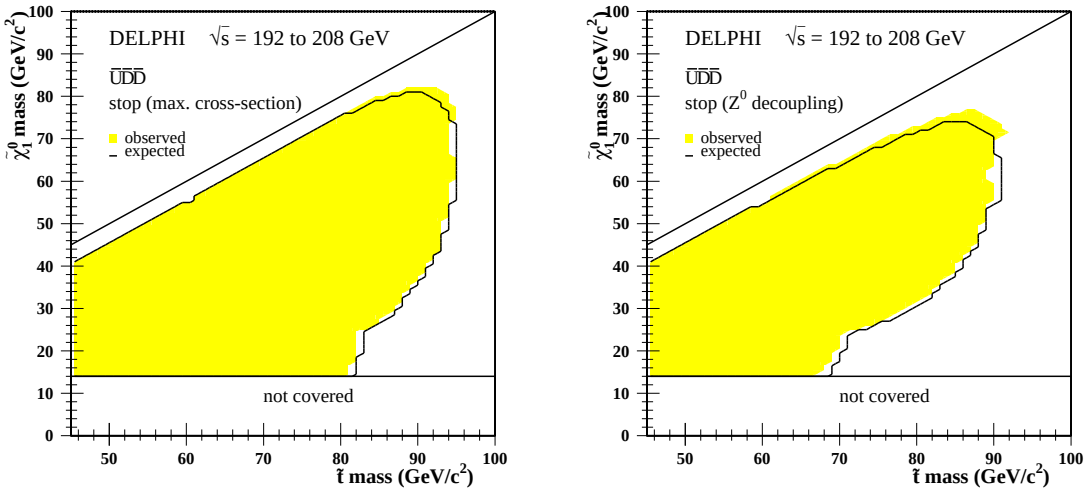

Figure 18: $\bar{U}\bar{D}\bar{D}$: exclusion domains at 95% CL in the $m_{\tilde{\chi}_1^0}$ versus $m_{\tilde{t}}$ plane for the stop pair-production, with BR($\tilde{t} \rightarrow c\tilde{\chi}_1^0$) = 100% and neutralino decay into jets. The plots show the exclusion (filled area) for the lightest stop for no mixing (left) and for the mixing leading to the maximal decoupling to the Z boson (right). The black contour is the corresponding expected exclusion at 95% CL.

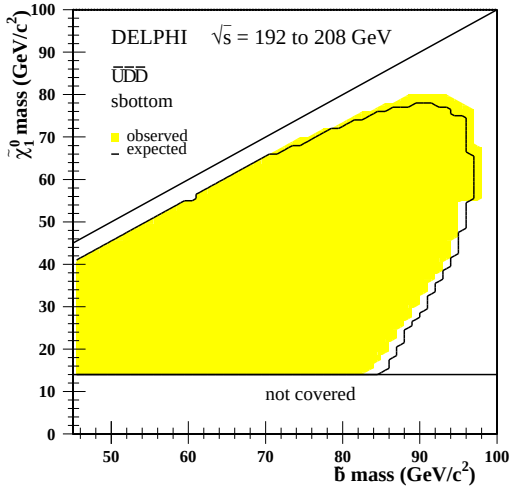

Figure 19: $\bar{U}\bar{D}\bar{D}$: exclusion contours at 95% CL in the $m_{\tilde{\chi}_1^0}$ versus $m_{\tilde{b}}$ plane for the sbottom pair-production, with BR($\tilde{b} \rightarrow b\tilde{\chi}_1^0$) = 100% and neutralino decay into jets. The plot shows the obtained exclusion (filled area) for the lightest sbottom in the case of no mixing. The black contour is the expected exclusion at 95% CL.